Miner Deposita (2015) 50:895–922
DOI 10.1007/s00126-014-0564-x

ARTICLE

Timing of porphyry (Cu-Mo) and base metal (Zn-Pb-Ag-Cu) mineralisation in a magmatic-hydrothermal system—Morococha district, Peru

Honza Catchpole · Kalin Kouzmanov · Aldo Bendezú · Maria Ovtcharova · Richard Spikings · Holly Stein · Lluís Fontboté

Received: 8 January 2014 / Accepted: 29 October 2014 / Published online: 14 February 2015

Abstract The Morococha district in central Peru is characterised by economically important Cordilleran polymetallic (Zn-Pb-Ag-Cu) vein and replacement bodies and the large Toromocho porphyry Cu-Mo deposit in its centre. U-Pb, Re-Os, and $^{40}Ar/^{39}Ar$ geochronology data for various porphyry-related hydrothermal mineralisation styles record a 3.5-Ma multi-stage history of magmatic-hydrothermal activity in the district. In the late Miocene, three individual magmatic-hydrothermal centres were active: the Codiciada, Toromocho, and Ticlio centres, each separated in time and space. The Codiciada centre is the oldest magmatic-hydrothermal system in the district and consists of a composite porphyry stock associated with anhydrous skarn and quartz-molybdenite veins. The hydrothermal events are recorded by a titanite U-Pb age at 9.3±0.2 Ma and a molybdenite Re-Os age at 9.26±0.03 Ma. These ages are indistinguishable from zircon U-Pb ages for porphyry intrusions of the composite stock and indicate a time span of 0.2 Ma for magmatic-hydrothermal activity. The small Ticlio magmatic-hydrothermal centre in the west of the district has a maximum duration of 0.3 Ma, ranging from porphyry emplacement to porphyry mineralisation at 8.04±0.14 Ma ($^{40}Ar/^{39}Ar$ muscovite cooling age). The Toromocho magmatic-hydrothermal centre has a minimum of five recorded porphyry intrusions that span a total of 1.3 Ma and is responsible for the formation of the giant Toromocho Cu-Mo deposit. At least two hydrothermal pulses are identified. Post-dating a first pulse of molybdenite mineralisation, widespread hydrous skarn covers an area of over 6 km^2 and is recorded by five $^{40}Ar/^{39}Ar$ cooling ages at 7.2–6.8 Ma. These ages mark the end of the slowly cooling and long-lived Toromocho magmatic-hydrothermal centre soon after last

Editorial handling: H.A. Gilg and G. Beaudoin

Electronic supplementary material The online version of this article (doi:10.1007/s00126-014-0564-x) contains supplementary material, which is available to authorized users.

H. Catchpole (✉) · K. Kouzmanov · A. Bendezú · M. Ovtcharova · R. Spikings · L. Fontboté
Department of Earth and Environmental Sciences, University of Geneva, Rue des Maraîchers 13, 1205 Geneva, Switzerland
e-mail: catchpole@gmx.de

K. Kouzmanov
e-mail: Kalin.Kouzmanov@unige.ch

A. Bendezú
e-mail: Aldobendezujuarez@yahoo.com

M. Ovtcharova
e-mail: Maria.Ovtcharova@unige.ch

R. Spikings
e-mail: Richard.Spikings@unige.ch

L. Fontboté
e-mail: Lluis.Fontbote@unige.ch

H. Stein
AIRIE Program, Department of Geosciences, Colorado State University, Fort Collins, CO 80523-1482, USA
e-mail: Holly.Stein@colostate.edu

H. Stein
Centre for Earth Evolution and Dynamics, University of Oslo, 0316 Oslo, Norway

Present Address:
H. Catchpole
Vale Exploration Canada Inc., 2060 Flavelle Boulevard, Mississauga, Ontario, Canada L5K 1Z9

magmatic activity at 7.26±0.02 Ma. District-wide (50 km^2) Cordilleran base metal vein and replacement bodies post-date the youngest recorded porphyry mineralisation event at Toromocho by more than 0.5 Ma. Polymetallic veins (5.78±0.10 and 5.72±0.18 Ma; ^{40}Ar/^{39}Ar ages) and the Manto Italia polymetallic replacement bodies (6.23±0.12 and 6.0±0.2 Ma; ^{40}Ar/^{39}Ar ages) are interpreted to have been formed by a single hydrothermal pulse. Hydrothermal activity ceased after the formation of the base metal vein and replacement bodies. Overlapping monazite U-Pb (8.26±0.18 Ma) and muscovite ^{40}Ar/^{39}Ar ages (8.1±0.5 Ma) from the early base metal stage of one Cordilleran vein sample in the Sulfurosa area provide evidence that a discrete hydrothermal pulse was responsible for polymetallic vein formation 2.6 Ma prior to the district-wide polymetallic veins. These ages pre-date those of Toromocho porphyry Cu-Mo formation and show that Zn-Pb-Ag-Cu mineralisation formed during several discrete magmatic-hydrothermal pulses in the same district.

Keywords ^{40}Ar/^{39}Ar geochronology · Zn-Pb-Ag-Cu · Morococha · Porphyry · Toromocho · Cordilleran polymetallic

Introduction

Mining districts with important porphyry-type Cu±Mo±Au as well as base and precious metal mineralisation (Zn-Pb-Cu-Ag-Au) usually have a protracted magmatic and hydrothermal history. They are characterised by the superposition of multiple magmatic and hydrothermal events over a time period as short as one hundred thousand years to several million years (Deckart et al. 2014; Harris et al. 2008; Masterman et al. 2004; Muntean and Einaudi 2000; Seedorff et al. 2005; Sillitoe and Mortensen 2010). Individual magmatic-hydrothermal systems can comprise a variety of different mineralisation styles, which may include porphyry mineralisation and alteration, skarn and various types of mesothermal (>300°) and epithermal (<300 °C) base and precious metal mineralisation (Guilbert and Park 1986), which can also be grouped by the term "porphyry Cu system", as suggested by Sillitoe (2010).

Late mesothermal and epithermal base and precious metal mineralisation in porphyry Cu systems contributed substantial amounts of Cu, Zn, Pb, Ag, or Au to large-scale deposits, e.g. enargite-bearing, main-stage veins at Chuquicamata (Faunes et al. 2005; Ossandón et al. 2001), stage 3 veins at Escondida (Ojeda 1986; Padilla Garza et al. 2001), the Victoria Cu-Zn-Au-Ag and Lepanto Cu-Au deposits, Philippines (Hedenquist et al. 1998, 2001), and Main Stage veins in Butte, USA (Meyer et al. 1968).

Precise geochronology of different mineralisation styles in such porphyry systems is key to understanding the timing and dynamics of these magmatic-hydrothermal systems, and the relationships between porphyry and Zn-Pb-Cu-Ag-Au mineralisation. The Morococha magmatic-hydrothermal system of central Peru (Figs. 1 and 2) comprises several mineralised porphyry stocks, Zn-Pb-Ag-Cu-bearing and barren skarn, massive pyrite bodies, and Zb-Pb-Ag-Cu vein and carbonate-replacement deposits (Bartos 1989; McLaughlin and Graton 1935; Petersen 1965).

We present the first U-Pb and ^{40}Ar/^{39}Ar age data for hydrothermal minerals interpreted to have precipitated with the sulphides in the base metal vein and replacement bodies and new Re-Os and ^{40}Ar/^{39}Ar ages for skarn and porphyry mineralisation at Morococha. These data are combined with an existing dataset of magmatic and hydrothermal ages at Morococha (Bendezú et al. 2012; Beuchat 2003; Catchpole 2011; Eyzaguirre et al. 1975; Kouzmanov et al. 2008) and reveal several magmatic-hydrothermal centres that are separated in time and space, recording a 3.5-Ma history of intrusive and hydrothermal activity for the Morococha district.

Geological setting

The Morococha district (11°35′S, 76°20′W) is located in central Peru (Fig. 1), ~150 km northeast of Lima at an altitude of 4,500 to over 5,000 m. The district lies in the Miocene metallogenic belt that extends along the Western Cordillera of northern and central Peru (Noble and McKee 1999; Petersen 1965). The hydrothermal deposits formed in this metallogenic belt are associated with subduction-related calc-alkaline magmatism, ranging in age from 6 to 20 Ma (Bissig et al. 2008; Noble and McKee 1999). Bissig et al. (2008) proposed that magmatism and deposit formation in the belt are related to flattening of the subducted slab at 14–11 Ma (Bissig and Tosdal 2009). Economic mineralisation found in the Miocene metallogenic belt includes porphyry-type Cu-Mo and Cu-Au deposits, as well as skarn and base and/or precious metal deposits.

The Morococha district is located in the northwestern sector of the Yauli Dome (Fig. 1). Paleozoic metasedimentary rocks of the Excelsior Group form the basement of the dome and are discordantly overlain by the Permo-Triassic Mitu Group, which dominates the central part of the dome structure (Beuchat 2003; Nagell 1960; Petersen 1965; Rivera and Kobe 1983; Terrones 1949). The heterogeneous Excelsior Group includes phyllites, lower Paleozoic shales, and quartzites which were deformed during the Variscan orogenesis (Lepry 1981). The Mitu Group comprises two main lithologies; red beds (conglomerates, sandstones, and shales) and volcanic rocks locally known as Catalina volcanics (alkaline lavas and pyroclastic flows), which probably have a continental origin with an extreme lateral variation in thickness (Mégard 1984; Rivera and Kobe 1983). Upper Triassic-Jurassic carbonate rocks of the Pucará Group, Cretaceous clastic rocks of the Goyllarisquizga Group, and Upper Cretaceous limestones

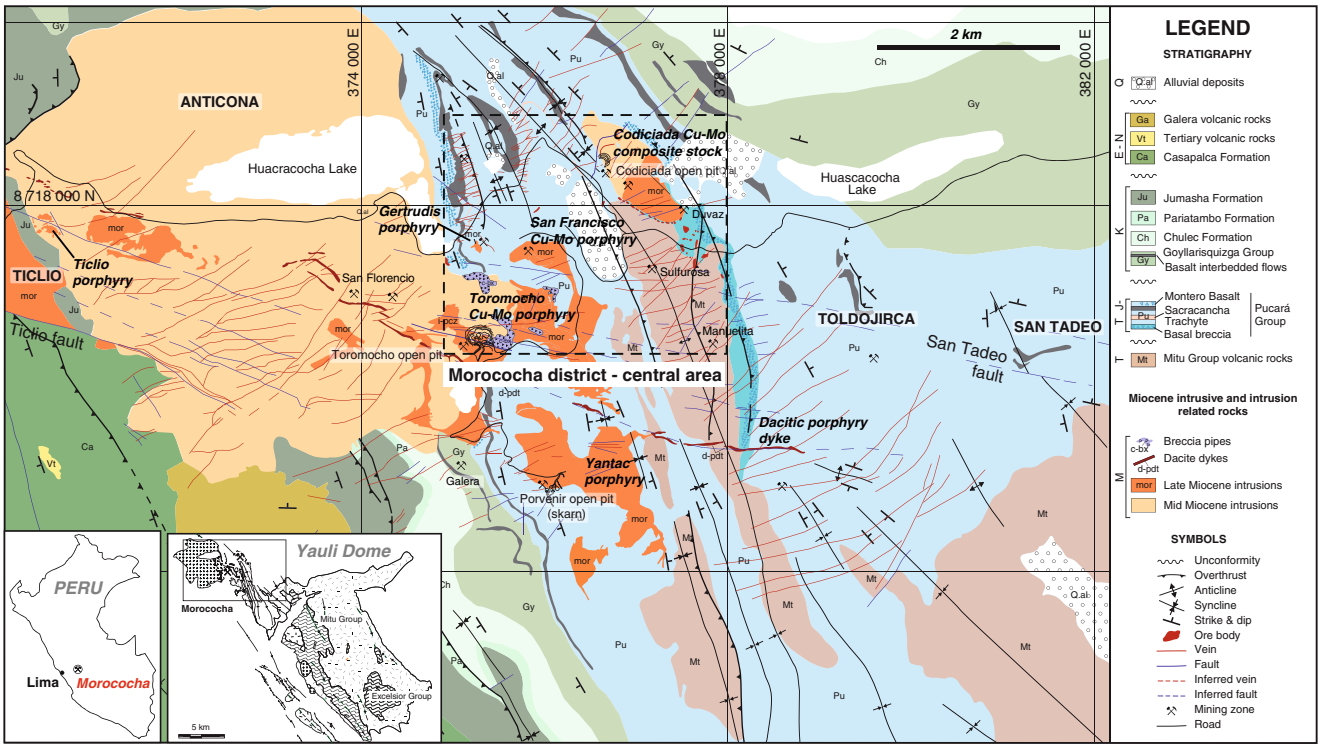

Fig. 1 Geologic map of the Morococha district, modified from Bendezú et al. (2008a), based on Lepry (1981) and Alvarez (1999), maps of the Cerro de Pasco Corporation (1965) and Centromin Peru (2002), and maps produced during this study

(Chulec, Pariatambo, Jumasha groups) discordantly overlie the Palaeozoic-Triassic rocks (Rosas et al. 2007). The Montero Basalt and Sacracancha Trachyte volcanic rocks are interlayered with carbonate rocks of the Pucará Group and record phases of volcanic activity. The Cretaceous Casapalca red beds discordantly overlie the Upper Cretaceous limestones. The Galera lavas and pyroclastic flows of rhyolitic composition unconformably overlie Upper Cretaceous limestones in the southern part of the district (Bendezú et al. 2012). The western part of the central Morococha district is characterised by the north-western extremity of a minor, north-northwestern striking anticline related to the Yauli Dome (Rivera and Kobe 1983).

Miocene porphyry intrusions

Multiple intrusions were emplaced into the Triassic-Jurassic Pucará Group carbonate rocks during the middle to late Miocene (Figs. 1 and 2; Bendezú et al. 2008a; 2012; Beuchat 2003; Eyzaguirre et al. 1975; Kouzmanov et al. 2008). Intrusive activity commenced with the emplacement of the Codiciada microdiorite at 14.31±0.04 Ma (Bendezú et al. 2012) and the Anticona diorite at 14.11±0.04 (Beuchat 2003) and 14.07±0.04 Ma (Kouzmanov et al. 2008). The Anticona diorite dominates a large section of the western part of the district (Fig. 1). After a gap of ~5 Ma, a series of dioritic, granodioritic, and quartz monzonitic porphyry stocks intruded into the sedimentary sequences and the Anticona diorite from 9.4 to 7.7 Ma (Bendezú 2014, personal communication; Bendezú et al. 2012; Beuchat 2003; Kouzmanov et al. 2008). These porphyry stocks (Fig. 1) are described as "Morococha intrusions" (Boggio 1980), and now comprise the Ticlio, San Francisco, Gertrudis, and Yantac intrusions, and the Codiciada and Toromocho composite stocks (Bendezú et al. 2008a; Beuchat 2003). A dacite porphyry dyke set is emplaced at 7.26±0.02 Ma (Kouzmanov et al. 2008). It cuts the entire Morococha district roughly trending east-southeast to west-northwest and is the youngest recorded magmatic event (Fig. 1, Table 1). All middle to late Miocene intrusions are calc-alkaline in composition (Kouzmanov et al. 2008).

Hydrothermal mineralisation styles

Porphyry-type mineralisation

The Anticona diorite and Codiciada microdiorite do not show any direct relationships with Miocene porphyry-type mineralisation. Porphyry-type veins and disseminated mineralisation occur in the Toromocho composite stock (Cu-Mo), the San Francisco porphyry intrusion (Cu-Mo), the Codiciada composite stock (Cu-Mo), the Sulfurosa area to

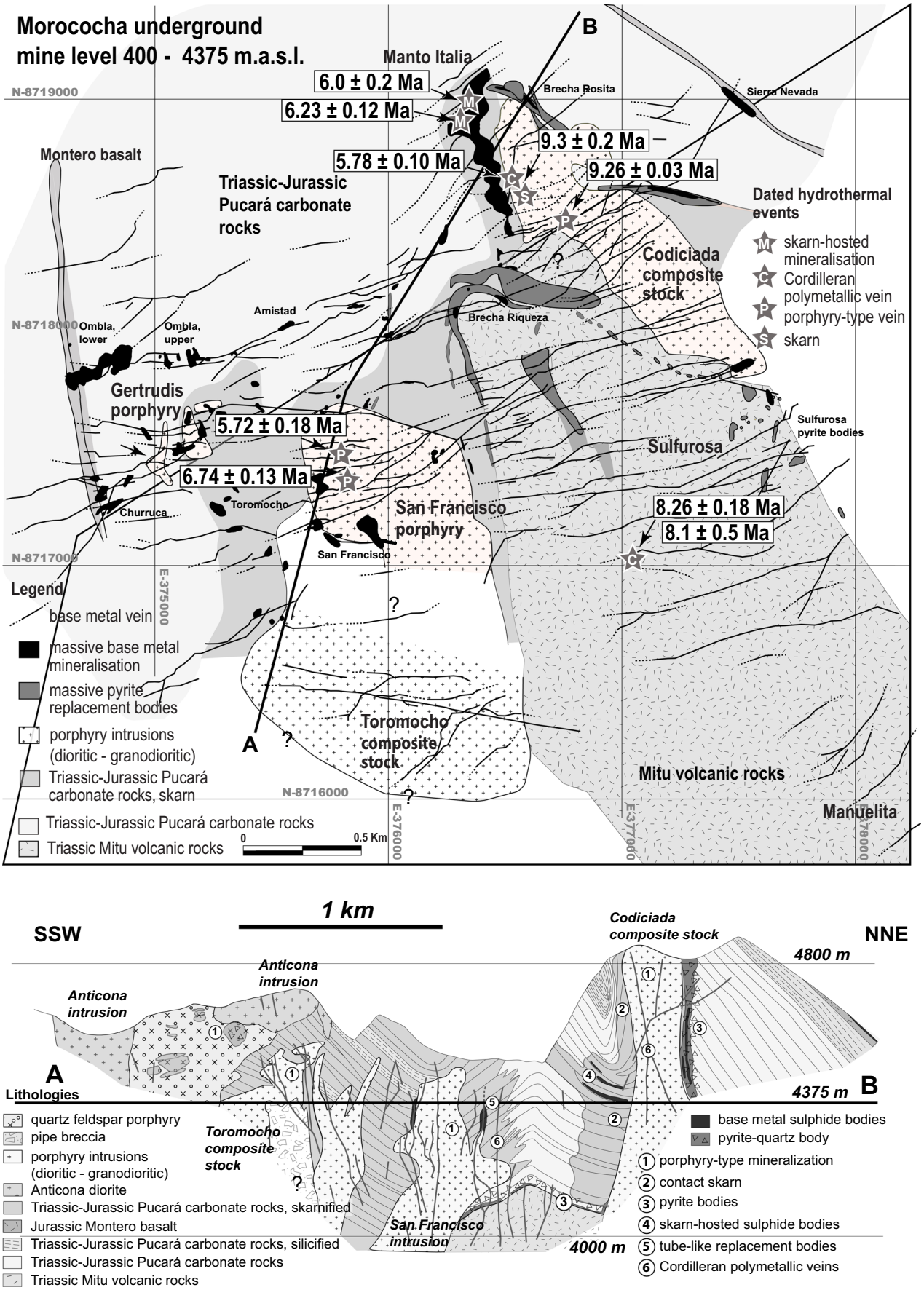
Morococha underground
mine level 400 - 4375 m.a.s.l.
Manto Italia
6.0 ± 0.2 Ma
6.23 ± 0.12 Ma
5.78 ± 0.10 Ma
9.3 ± 0.2 Ma
9.26 ± 0.03 Ma
Brecha Rosita
Sierra Nevada
Montero basalt
Triassic-Jurassic
Pucará carbonate
rocks
Dated hydrothermal
events
skarn-hosted
mineralisation
Cordilleran
polymetallic vein
porphyry-type vein
skarn
Codiciada
composite
stock
Brecha Riqueza
Amistad
Ombla,
lower
Ombla,
upper
Gertrudis
porphyry
5.72 ± 0.18 Ma
6.74 ± 0.13 Ma
Sulfurosa
pyrite bodies
Sulfurosa
Churruca
Toromocho
San Francisco
porphyry
8.26 ± 0.18 Ma
8.1 ± 0.5 Ma
San Francisco
Legend
base metal vein
massive base metal
mineralisation
massive pyrite
replacement bodies
porphyry intrusions
(dioritic - granodioritic)
Triassic-Jurassic Pucará
carbonate rocks, skarn
Toromocho
composite
stock
Mitu volcanic rocks
Manuelita
Triassic-Jurassic Pucará carbonate rocks
Triassic Mitu volcanic rocks
0
0.5 Km
N-8719000
N-8718000
N-8717000
N-8716000
E-375000
E-376000
E-377000
E-378000
A
B
1 km
SSW
NNE
Codiciada
composite stock
4800 m
Anticona
intrusion
Anticona
intrusion
4375 m
Lithologies
quartz feldspar porphyry
pipe breccia
porphyry intrusions
(dioritic - granodioritic)
Anticona diorite
Triassic-Jurassic Pucará carbonate rocks, skarnified
Jurassic Montero basalt
Triassic-Jurassic Pucará carbonate rocks, silicified
Triassic-Jurassic Pucará carbonate rocks
Triassic Mitu volcanic rocks
Toromocho
composite
stock
San Francisco
intrusion
4000 m
base metal sulphide bodies
pyrite-quartz body
1 porphyry-type mineralization
2 contact skarn
3 pyrite bodies
4 skarn-hosted sulphide bodies
5 tube-like replacement bodies
6 Cordilleran polymetallic veins

◀ **Fig. 2** Geological map of mining level 400 (4,375 m a.s.l.) showing the distribution of mineralised bodies (compiled and projected from multiple mining levels) and schematic cross-section in the central Morococha district, compiled from geological maps of the Cerro de Pasco Copper Corp. (1920–1960), Centromin Peru, Pan American Silver Corp. and León Pimentel (2006). The vertical exaggeration is 1.8. New radiogenic isotope ages (this study) for different mineralisation types are reported and different mineralisation styles are indicated by *numbers 1–6* in the profile

the southeast of Toromocho, and the Ticlio porphyry intrusion (Cu-Au) in the far west of the district (Fig. 1).

The giant Toromocho porphyry Cu-Mo deposit occupies the central part of Morococha and is the only currently economic porphyry-type deposit in the district. Proven and probable reserves are reported to be 1.37 Gt at 0.51 % Cu, 0.018 % Mo, and 7.06 g/t Ag (Alvarez 1999; Lowell and Alvarez 2005; Peru Copper Inc. 2006). Extensive potassic and phyllic alteration zones host a stockwork mineralisation of quartz-chalcopyrite±chalcocite, quartz-pyrite and chalcocite, and quartz-pyrite-molybdenite veinlets. Chalcocite results from supergene enrichment processes. Disseminated Cu mineralisation associated with potassic alteration is common for hydrothermal breccia pipes in the central part of the deposit.

At least two hydrothermal pulses have been identified. One caused economic mineralisation at 8.0–7.8 Ma (7.97±0.11 and 7.77±0.11 Ma, Re-Os; Beuchat 2003) and one is recorded by biotite cooling ages at 7.2±0.3 (K-Ar; Eyzaguirre et al. 1975) and 6.81±0.14 Ma ($^{40}Ar/^{39}Ar$; Kouzmanov et al. 2008).

The Codiciada composite stock displays strong Na-Ca alteration and moderate potassic alteration, which are overprinted by sericitic alteration. Sub-economic porphyry-type quartz-pyrite-chalcopyrite±pyrrhotite and quartz-molybdenite veins are cut by later Cordilleran polymetallic veins (Figs. 3a and 4).

The small Ticlio porphyry in the western part of the district displays a zoned mineralisation and alteration pattern. A core of high-density stockwork of quartz-magnetite±K-feldspar veins changes progressively to an outer zone of intense K-feldspar alteration with a low-density of magnetite and quartz-magnetite veinlets that host small amounts of bornite and native Au inclusions in chalcopyrite. An outermost zone displays a strong pyrite-quartz-sericitic alteration and skarn mineralisation in adjacent Cretaceous carbonate rocks (Bendezú et al. 2008a; Chevalier 2010).

Skarn mineralisation

Skarn mineralisation in the Morococha district is spatially associated with several porphyry intrusions: the Codiciada composite stock, the Gertrudis stock, the San Francisco stock (Catchpole 2011; McLaughlin and Graton 1935; Petersen 1965), the Yantac stock (Beuchat 2003), the Toromocho composite stock (Alvarez 1999; Lowell and Alvarez 2005), and the Ticlio stock (Chevalier 2010). Phlogopite $^{40}Ar/^{39}Ar$ ages for skarn adjacent to intrusive bodies at several locations in the district reveal at least two and perhaps three individual skarn forming events within a period of 1.9 Ma: 8.81±0.18 Ma for the Codiciada skarn (Kouzmanov et al. 2008), 7.2±0.2 Ma for the Porvenir skarn adjacent to the Yantac intrusions (Beuchat 2003), and a 6.9±0.3 Ma for the Gertrudis skarn (Catchpole 2011). Dolomites and dolomitic limestones of the Pucará Group are replaced by magnesian serpentine-magnetite±phlogopite and tremolite-diopside-serpentine-chlorite-talc exoskarn and calcic andradite-diopside-epidote exoskarn. There are smaller occurrences of grossular-diopside endoskarn and spinel-bearing diopside-grossular endoskarn that replaced Miocene porphyries at the contact with Pucará Group carbonate rocks (Catchpole 2011). Economically important polymetallic (Zn-Pb-Ag-Cu) mineralisation is hosted in exoskarn dominated by hydrous skarn mineral assemblages or is found as skarn-free carbonate-replacement bodies in the carbonate rocks of the Pucará Group (Fig. 3b, c). Massive Zn-Pb-Ag-Cu-bearing sulphide bodies discovered in the Manto Italia are up to 20 m thick and located adjacent to the Codiciada composite stock (Fig. 2; Catchpole 2011; Paliza and Chavez 2008). The most abundant sulphides are pyrrhotite, pyrite, chalcopyrite, sphalerite, and galena (Figs. 3b, c). Outer zones of these bodies are marked by anhydrous diopside-andradite skarn assemblages, and the inner zones by later hydrous tremolite-serpentine-chlorite-talc skarn and sulphide assemblages (Catchpole 2011). A detailed paragenetic sequence is provided in Fig. 5.

Pyrite bodies

Massive pyrite replacement bodies are found in several underground and surface locations in the central Morococha district (Fig. 3d, e). They are essentially barren, but are economically interesting where later Cordilleran polymetallic veins (Fig. 3f, g) cross-cut and introduce Zn-Pb-Ag-Cu sulphides (e.g. Brecha Rosita, northern Codiciada; Brecha Riqueza, central Morococha: Figs. 2 and 3f, g). All pyrite bodies replace fractured and deformed Pucará Group carbonate host rocks. The massive pyrite bodies develop mainly (a) along the contact of volcanic rocks of the Mitu Group with brecciated carbonate rocks of the Pucará Group (e.g. Brecha Riqueza), and (b) along the contact of porphyry intrusions with brecciated carbonate rocks (e.g. Brecha Rosita, see profile in Fig. 2). Vertical to sub-vertical tube-like pyrite bodies also form along steeply dipping fault structures (e.g. lower section of the Ombla body, see below). The pyrite bodies can have a banded texture of coarse- and fine-grained layers of pyrite, possibly mimicking former carbonate layers (Fig. 3e). Pyrite bodies are usually composed of about 80–90 vol% pyrite, while the remainder is quartz and accessory amounts

Table 1 Published age data from the Morococha district

Area	Intrusion/mineralisation	Mineral	Dating method				Age (Ma)	Source
			U-Pb	$^{40}Ar/^{39}Ar$	Re-Os	K-Ar		
Intrusive magmatic events:								
Codiciada	Microdiorite	Zircon	x				14.31±0.04	Bendezú et al. (2012) [a]
Anticona	Diorite-Ticlio area	Zircon	x				14.11±0.04	Beuchat (2003)
Anticona	Diorite-SW sector	Zircon	x				14.07±0.04	Kouzmanov et al. (2008)
Codiciada	Aplitic dyke cutting microdiorite	K-feldspar		x			9.5±0.2	Bendezú et al. (2012) [a]
Codiciada	Hornblende-porphyry	Zircon	x				9.30±0.03	Bendezú et al. (2012) [a]
Codiciada	Quartz-feldspar porphyry	Zircon	x				9.29±0.01	Bendezú et al. (2012) [a]
San Francisco	San Francisco porphyry	Zircon	x				9.42±0.17	Bendezú et al. (2012) [a]
San Francisco	San Francisco porphyry	Zircon	x				9.11±0.10	Beuchat (2003)
Ticlio	Ticlio granodiorite	Zircon	x				8.31±0.03	Bendezú et al. (2012) [a]
Yantac	Yantac porphyry	zircon	x				8.81±0.06	Beuchat (2003)
Yantac	Yantac porphyry	Biotite		x			8.4±0.4	Bendezú et al. (2012) [a]
Yantac	Yantac porphyry	Biotite				x	8.3±0.3	Eyzaguirre et al. (1975)
Yantac	Yantac porphyry	K-feldspar		x			8.01±0.12	Bendezú et al. (2012) [a]
Toromocho	Granodiorite porphyry	Zircon	x				8.45±0.05	Kouzmanov et al. (2008)
Toromocho	Feldspar porphyry	Zircon	x				7.73±0.02	Kouzmanov et al. (2008)
Toromocho	Quartz porphyry	Zircon	x				7.75±0.13	Kouzmanov et al. (2008)
Toromocho	Dacitic porphyry dyke	Zircon	x				7.26±0.02	Kouzmanov et al. (2008)
Anticona	Dyke cutting Anticona diorite	Magmatic biotite				x	8.2±0.2	Eyzaguirre et al. (1975)
Porphyry type mineralisation:								
Toromocho	Quartz-molybdenite veins cutting quartz porphyry	Molybdenite			x		7.97±0.11	Beuchat (2003)
Toromocho		Molybdenite			x		7.77±0.11	Beuchat (2003)
Toromocho	Hydrothermal biotite	Hydrothermal biotite				x	7.2±0.3	Eyzaguirre et al. (1975)
Toromocho	Quartz-biotite vein cutting granodiorite porphyry	Biotite		x			6.81±0.14	Kouzmanov et al. (2008)
Skarn type mineralisation:								
Codiciada	Codiciada hydrous skarn	Phlogopite		x			8.81±0.18	Kouzmanov et al. (2008)
Gertrudis	Gertrudis hydrous skarn	Phlogopite		x			6.9±0.3 [b]	Catchpole (2011)
Gertrudis	Gertrudis hydrous skarn	Phlogopite		x			6.42±0.19 [c]	Beuchat (2003)
Yantac	Porvenir hydrous skarn	Phlogopite		x			7.2±0.2	Beuchat (2003)

Reported U-Pb dates are concordant and $^{40}Ar/^{39}Ar$ dates are plateau dates except where indicated

[a] Bendezú et al. (2012) and Bendezú (2014) personal communication

[b] New age for Gertrudis skarn that replaces older minimum age by Beuchat (2003)

[c] Not a weighted mean plateau and interpreted as minimum age

of rutile. Porphyry intrusive and volcanic rocks in contact with the pyrite bodies show intense sericitic and chlorite alteration. The pyrite bodies are similar to the massive pyrite bodies that characterise the Miocene base metal deposit Cerro de Pasco, Peru (Baumgartner et al. 2008).

Cordilleran polymetallic veins and replacement bodies

Steeply dipping Zn-Pb-Ag-Cu-bearing Cordilleran base metal veins with sericitic alteration halos are hosted by mainly NNE to ENE striking faults, and cut intrusive bodies, surrounding sedimentary rocks, pyrite bodies, and skarn at the district scale (Catchpole et al. 2011, 2012, 2015; Petersen 1965). Their vertical extent exceeds 1 km, and ranges from altitudes of about 5,100 m at the highest points of the district to the lowest mining levels at 4,000 m (Fig. 2). Carbonate replacement bodies are vertical chimneys at the contact of intrusive bodies with carbonate beds, and mantos and irregular bodies along fault zones. These massive sulphide bodies form where Cordilleran base metal veins intercept faults or lithological

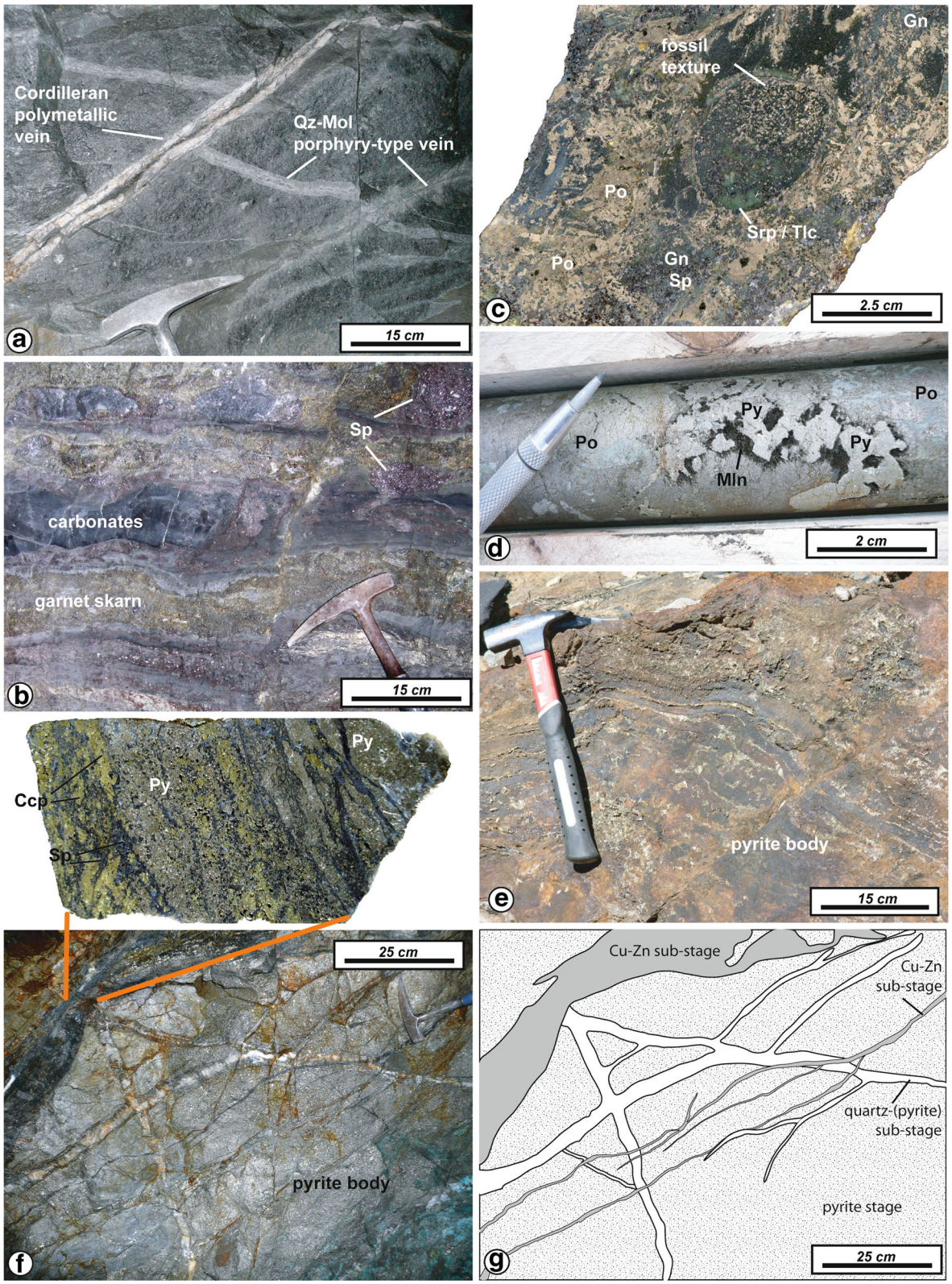

Fig. 3 Hydrothermal mineralisation types and cross-cutting relationships in the central Morococha district: **a** carbonate-rich Cordilleran polymetallic vein cutting and displacing earlier porphyry quartz-molybdenite vein hosted by the Codiciada microdiorite with potassic alteration; **b** Manto Italia polymetallic replacement bodies: Pucará Group carbonates interlayered with andradite and dark red sphalerite; **c** polished slabs of fossil-bearing carbonate layers replaced by hydrous skarn and sulphide assemblage; **d** massive pyrrhotite from Manto Italia drill core being replaced by melnikovite and idiomorphic pyrite; **e** banded, coloform replacement patterns of former carbonate layers by massive pyrite; **f**, **g** massive pyrite body cross-cut by Cordilleran polymetallic veins, resolved into sub-stages in the schematic diagram. *Ccp* chalcopyrite, *Gn* galena, *Mln* melnikovite, *Mol* molybdenite, *Po* pyrrhotite, *Py* pyrite, *Qz* quartz, *Srp* serpentine, *Sp* sphalerite, *Tlc* talc

contacts that act as conduits for hydrothermal fluid. Examples are the Cu-rich replacement bodies in the central area, near the San Francisco and Gertrudis intrusion, e.g. the Ombla, Toromocho, Churruca, and Amistad ore bodies in Fig. 2 (Catchpole et al. 2015; Cerro de Pasco Copper Corporation 1948; McLaughlin and Graton 1935; Trefzger 1937). These ore bodies were mostly mined before 1970.

The veins are internally well zoned and can be subdivided into three stages based on cross-cutting relationships (Catchpole et al. 2011). The first stage is characterised by barren quartz-pyrite with sericitic alteration halos. Zn-Pb-Ag-Cu sulphides are introduced during the composite, second base metal stage, and abundant pink rhodochrosite and quartz mark the last carbonate stage (Fig. 4). The base metal stage can be further subdivided into several sub-stages. Stages and sub-stages can be discrete within a single vein (Fig. 4), or by contrast, be presented as individual veins with clear cross-cutting relationships, e.g. where veinlets cut massive pyrite bodies (Fig. 3f, g). The most abundant base metal sulphides are sphalerite, galena, tennantite-tetrahedrite, chalcopyrite, and enargite. Silver is mostly present as a trace or minor element in tennantite-tetrahedrite and as Ag-telluride (hessite), whereas galena is mostly poor in Ag. A generalised mineral paragenesis showing the position of the minerals dated is presented in Fig. 6.

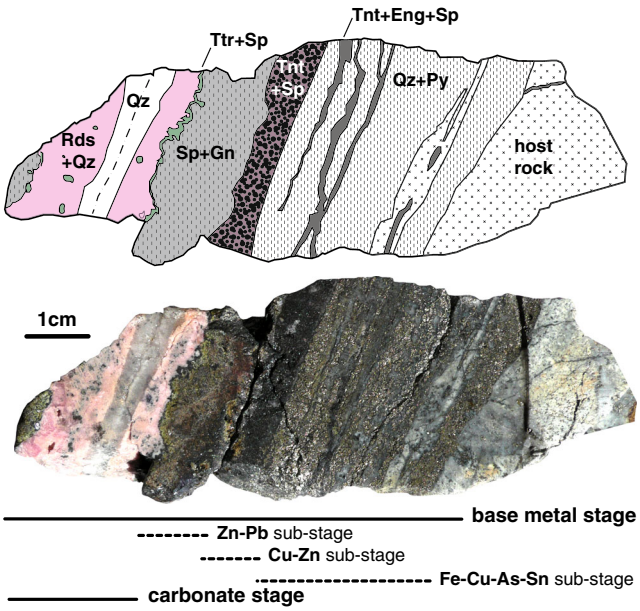

Fig. 4 Core to rim polished slab of a well zoned Cordilleran polymetallic vein with quartz-pyrite and base metal stage, including various sub-stages (Catchpole et al. 2011, 2015); A schematic sketch shows the main mineral zones with mineral assemblages. *Ccp* chalcopyrite, *Eng* enargite, *Gn* galena, *Py* pyrite, *Qz* quartz, *Rds* rhodochrosite, *Sp* sphalerite, *Tnt* tennantite, *Ttr* tetrahedrite

Methodology

Sample preparation

Mineral samples used for geochronology were either hand-picked from vugs or separated from bulk rock using detailed crushing and separation protocols that are described in Electronic Supplementary Material (ESM) 1. Descriptions of the mineral separates are summarised in Table 2. All mineral separates analysed by the infrared (CO_2) laser $^{40}Ar/^{39}Ar$ method were tested for purity by powder X-ray diffraction of a crushed aliquot of each grain separate (Philips X'Pert APD, University of Geneva). Additional aliquots were used for thin section grain mounts of ~20–40 grains of each sample and checked for alteration textures and compositional inhomogeneities using scanning electron microscope backscatter electron imaging (SEM-BSE; CamScan4, University of Lausanne). Representative grain compositions were subsequently quantified by electron microprobe analysis (Table 3).

U-Pb analytical methods

Monazite and titanite samples were fluxed in 3 N HNO_3 in Savillex vials and rinsed in distilled water and acetone in an ultrasonic bath. After adding a mixed ^{205}Pb-^{233}U-^{235}U spike to the samples (EARTHTIME, spike calibration described by Condon et al. 2010) single to multi-grain fractions of monazites and titanites were selected, weighed, and loaded for dissolution in 6 N HCL (monazite) and concentrated HF with a trace of 7 N HNO_3 (titanite). After evaporation and overnight redissolution in 6 N HCl the titanite samples were brought up in 1 N HBr. Following Pb and U separation (Krogh 1973), U-Pb geochronology was performed using isotope dilution thermal ionisation mass spectrometry (ID-TIMS) at the University of Geneva on a TRITON mass spectrometer equipped with a linear MasCom electron multiplier. Age calculations are based on the decay constants of Jaffey et al. (1971). The initial statistics was done using the TRIPOLI program (Bowring et al. 2011), followed by data reduction and age calculation using the YourLab xls program (Schmitz and Schoene 2007). All uncertainties are reported at 2 sigma level. Details of the analytical method are presented in ESM 1.

Re-Os analytical methods

Isotopic ratios were measured by negative thermal ion mass spectrometry on a Triton machine housed within the AIRIE Program at Colorado State University. The Re-Os data for the molybdenite were acquired using a Carius tube dissolution and a mixed Re-double Os spike (Markey et al. 2003). The double Os spike is useful for working with young and/or low Re molybdenites or sulphides with molybdenite-like isotopic compositions and allows determination and correction for

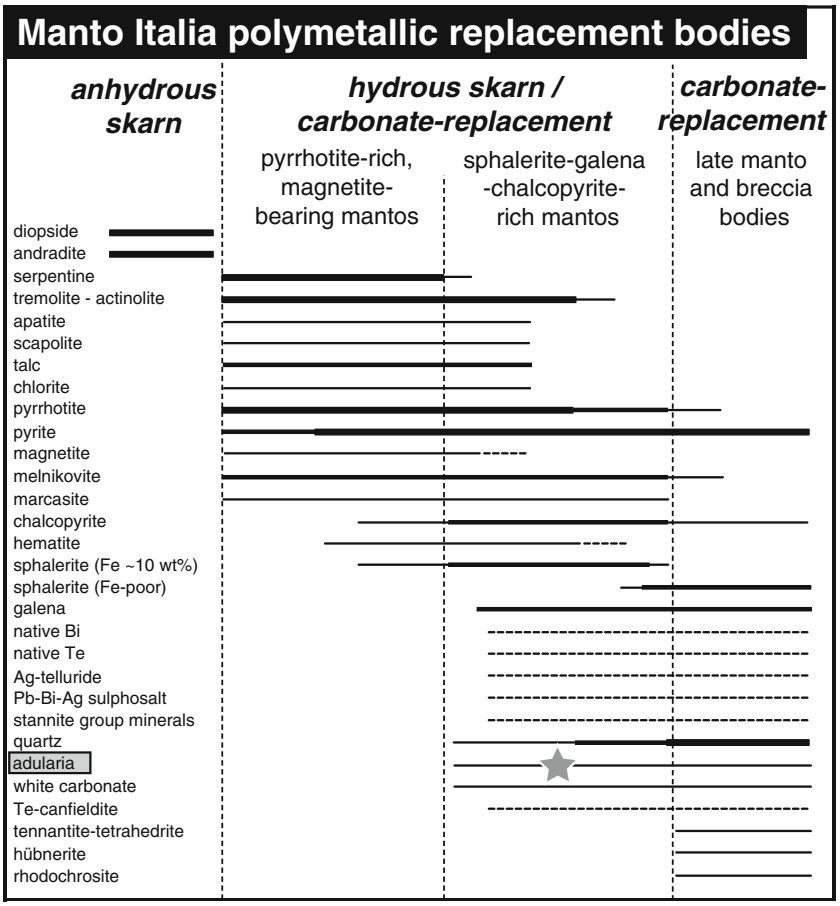

Fig. 5 Generalised mineral paragenesis of Manto Italia polymetallic replacement bodies. *Thick bars* indicate higher abundances and *dashed lines* indicate lesser abundances. *Stars* indicate the paragenetic position of the adularia and muscovite that were dated by $^{40}Ar/^{39}Ar$ and the monazite dated by U-Pb

common Os as well as a mass fractionation correction for measured Os isotope ratios (Stein et al. 2001). The Re-Os data for two analysed pyrites were acquired via the same method, but using single ^{185}Re and ^{190}Os spikes (Stein et al. 2000). Analytical details of the sample preparation and dating method are presented in the ESM 1.

Infrared (CO_2) laser $^{40}Ar/^{39}Ar$ analysis

Samples for $^{40}Ar/^{39}Ar$ analysis were loaded into Cu foil packages and mounted inside a silica glass tube. Fish Canyon Tuff sanidine was added as a flux monitor assuming a standard age of 28.02±0.28 Ma (Renne et al. 1998). The tube was irradiated for 3 h in the cadmium-lined in-core irradiation tube facility of the TRIGA reactor at the Oregon State University Radiation Center, USA. Analyses was performed via incremental heating using a MIR10 IR 30 W CO_2 laser and a stainless steel extraction line coupled with a multi-collector Argus mass spectrometer (GV Instruments), housed at the University of Geneva. The samples were placed in small pits in a Cu planchette and step-heated by laser rastering the pit area to ensure even-heating of the grains. Usual degassing consisted of 9–15 temperature steps. Blanks for all argon isotopes were measured at the beginning of a sample measurement and after every second step incremental heating experiment. Age plateaus were determined using the criteria of Dalrymple and Lanphere (1971), which specify the presence of at least three contiguous incremental heating steps with concordant ages that constitute >50 % of the total ^{39}Ar released during the step-heating experiment. All ages were calculated using decay constants and isotopic compositions of Steiger and Jäger (1977). Analytical details of the sample preparation and dating method are presented in the ESM 1.

Electron probe micro-analysis

Electron Probe Micro-Analysis was performed with a JEOL 8200 Superprobe electron microprobe at the University of Lausanne and operated at an acceleration potential of 15 kV, a probe current of 15 nA, and with a beam diameter of 5 μm. The compositions of muscovite and adularia were determined using following standards (Kα, if not otherwise specified): orthoclase for Si and K, albite for Al and Na, bytownite for Ca, diopside for Mg, orthopyroxene for Fe, $MnTiO_3$ for Ti and Mn, apatite for F, scapolite for Cl, and SnS for Sn (Lα). The

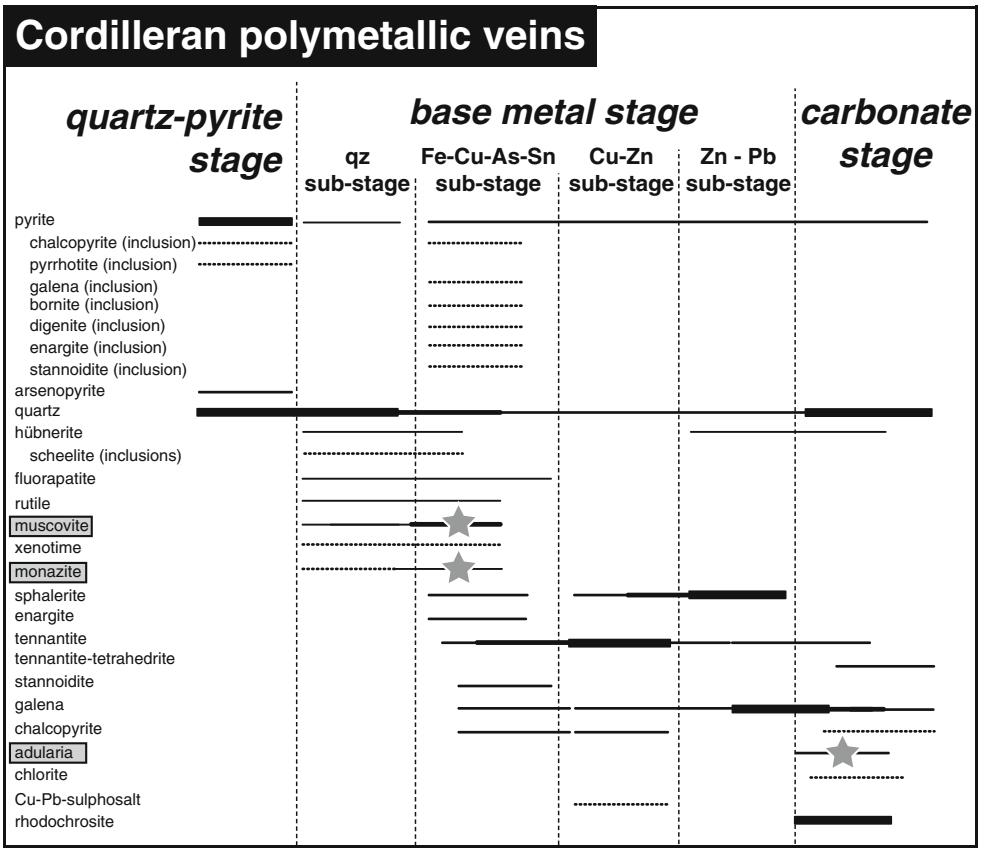

Fig. 6 Generalised mineral paragenesis of the Cordilleran polymetallic veins. *Thick bars* indicate higher abundances and *dashed lines* indicate lesser abundances. *Stars* indicate the paragenetic position of the adularia and muscovite that were dated by $^{40}Ar/^{39}Ar$ and the monazite dated by U-Pb

counting times were 10 s for K, Na, Ca, F, and Cl, and 20 s for the other elements.

Petrography of geochronology samples

Porphyry and skarn mineralisation

Titanite is found in diopside-rich, grey skarn (KMO-6-236) that replaces potassic-altered, biotite-rich volcaniclastic rocks that border the Codiciada microdiorite in the Codiciada open pit (Table 2). Titanite-bearing diopside-albite-actinolite veinlets with selvages of albite and actinolite (Na-Ca alteration) cut the microdiorite near the contact with the diopside skarn (Fig. 7a, b, c). Titanite is thus considered to be coeval with porphyry Na-Ca alteration and anhydrous diopside skarn mineralisation in the Codiciada area (Bendezú et al. 2008a).

A molybdenite sample was collected from a porphyry quartz-molybdenite vein cutting sericitic altered Codiciada microdiorite (KMO-6-407), in a location where several veins of this type are cross-cut by the Cordilleran polymetallic veins. The molybdenite occurs as millimeter-size grains locally intergrown with pyrite.

Two muscovite samples, KMO-8-203 and KMO-8-414, were extracted from vugs in milky quartz-rich veins that cut the San Francisco intrusion in the first underground mining level 122 (Fig. 8a). The veins predate Cordilleran polymetallic mineralisation. Large, 1–1.5-mm muscovite flakes (T-18) were collected from zones of strong sericitic alteration in the Ticlio porphyry (Fig. 8b). All samples have nearly pure muscovite composition with a small phengitic component. Muscovite samples KMO-8-203 and KMO-8-414 contain ~0.3–0.5 wt% F. Representative electron microprobe analyses are presented in Table 3.

Manto Italia polymetallic replacement bodies

Two adularia samples (KMO-6-308; KMO-6-306) were taken from massive sulphide mineralisation of the Manto Italia polymetallic replacement bodies hosted in fine-grained diopside skarn (Fig. 8c). Adularia is introduced late in the paragenetic sequence of polymetallic manto formation (Catchpole et al. 2015). Adularia-carbonate-galena veinlets cross-cut most other sulphides and skarn (Fig. 8d). Adularia is mostly idiomorphic and the crystals have a well-developed rhombic habit. Representative electron microprobe analyses are presented in Table 3.

Cordilleran polymetallic veins

Hydrothermal monazite and other accessory phosphates such as fluor-apatite and xenotime precipitate during the early base

Table 2 Description of geochronology samples from the Morococha district

Sample	Area	Location	UTM Coordinates		Mineralisation	Comment	Grain size (mm)	Mineral	Dating method
			N	E					
Porphyry and skarn type mineralisation									
KMO-6-407	Codiciada	Veta 2 vein, mine level 575	8718535	376735	Porphyry-style quartz-molybdenite vein	later phyllic alteration halo	–	Molybdenite	Re-Os
KMO-6-236	Codiciada	Codiciada open pit	8718417	376645	Anhydrous skarn stage/porphyry type Ca-Na alteration	Fine grained greenish-grey diopside skarn	0.08–0.15	Titanite	U-Pb
KMO-8-414	San Francisco	San Francisco mine level 122	8717392	376071	Porphyry style quartz vein	Crystals extracted from vugs in a 15 cm thick massive quartz vein with no sulphides present	0.5–1	Muscovite	$^{40}Ar/^{39}Ar$
KMO-8-203	San Francisco	San Francisco mine level 122	8717500	376400	Porphyry style quartz-pyrite-molybdenite vein	Crystals extracted from big vugs	0.2–0.5	Muscovite	$^{40}Ar/^{39}Ar$
T-18	Ticlio	Ticlio porphyry, surface outcrop	8717670	370620	Porphyry type phyllic alteration	Big crystals in strongly altered porphyry rock	1–1.5	Muscovite	$^{40}Ar/^{39}Ar$
Manto Italia polymetallic replacement bodies									
KMO-6-306	Manto Italia	Mining level 375	8718661	376420	Massive sulphide manto bodies with abundant hydrous skarn	Late polymetallic stage, together with galena and carbonates, post-dating skarn formation	0.2–0.4	Adularia	$^{40}Ar/^{39}Ar$
KMO-6-308	Manto Italia	Mining level 375	8718661	376420			0.2–0.4	Adularia	$^{40}Ar/^{39}Ar$
Pyrite body									
KMO-7-244	Sulfurosa	Sulfurosa, surface outcrop	8717588	377481	90 % pyrite, 10 % acicular quartz	Predating Cordilleran polymetallic veins	4	Pyrite	Re-Os
Cordilleran polymetallic vein									
KMO-6-102	Codiciada	San Andrés vein	8715994	378346	Early quartz-pyrite stage	Gangue minerals in the polymetallic vein hosted in andesites of the Mitu Group, except for sample KMO-6-273 hosted in Codiciada microdiorite	4	Pyrite	Re-Os
KMO-7-241	Sulfurosa	Veta Jackeline, level 750–230E, 4,310 m	8717220	377420	Early polymetallic stage		0.05–0.1	Monazite	U-Pb
KMO-7-241	Sulfurosa				Early polymetallic stage		0.1–0.3	Muscovite	$^{40}Ar/^{39}Ar$
KMO-6-273	Codiciada	Codiciada open pit	8718458	376629	Late Carbonate stage		0.1–0.2	Adularia	$^{40}Ar/^{39}Ar$
KMO-6-100	Manuelita	San Andrés vein	8715992	378311	Late Carbonate stage		0.3–1	Adularia	$^{40}Ar/^{39}Ar$

Table 3 Representative electron microprobe analyses of muscovite and adularia

Sample	KMO-8-203_ms_2	KMO-8-203_ms_3	KMO-8-414_ms_1-1	KMO-8-414_ms_1-3	T18_ms_1-1	KMO-6-273-adu_2-1	KMO-6-102-6_adu_2	KMO-6-308a_adu_1-1	KMO-6-308a_adu_1-2
Mineral	Muscovite	Muscovite	Muscovite	Muscovite	Muscovite	Adularia	Adularia	Adularia	Adularia
SiO2 (wt %)	47.62	47.92	48.18	49.39	48.48	65.10	65.30	65.87	65.69
TiO2	n.d.	n.d.	n.d.	n.d.	0.13	n.d.	n.d.	n.d.	n.d.
Al2O3	36.66	36.29	36.79	36.09	36.71	18.48	18.18	18.46	18.43
FeO	0.30	0.32	0.28	0.27	0.25	n.d.	n.d.	n.d.	n.d.
MgO	0.86	0.84	0.48	0.20	0.32	n.d.	n.d.	n.d.	n.d.
Na2O	0.21	0.23	0.20	n.d.	0.16	0.12	0.43	0.31	0.28
K2O	10.50	10.53	10.88	9.53	9.72	16.54	16.07	15.88	16.11
CaO	n.d.	n.d.	n.d.	n.d.	0.06	n.d.	n.d.	n.d.	n.d.
BaO	n.a.	n.a.	n.a.	n.a.	n.a.	n.a.	0.24	n.a.	n.a.
F-	0.39	0.30	0.46	0.34	n.d.	n.a.	n.a.	n.a.	n.a.
O=F	0.17	0.13	0.19	0.14	n.d.	–	–	–	–
Total	96.38	96.30	97.08	95.68	95.83	100.24	100.22	100.53	100.52
Si (apfu)	6.22	6.26	6.25	6.42	6.31	12.00	12.04	12.06	12.05
Ti	–	–	–	–	0.01	–	–	–	–
Al	1.78	1.74	1.75	1.58	1.69	4.02	3.95	3.98	3.98
Al	3.86	3.84	3.88	3.95	3.93	–	–	–	–
Fe2+	0.03	0.03	0.03	0.03	0.03	–	–	–	–
Mg	0.17	0.16	0.09	0.04	0.06	–	–	–	–
Ba	–	–	–	–	–	–	0.02	–	–
Ca	–	–	–	–	0.01	–	–	–	–
Na	0.05	0.06	0.05	–	0.04	0.04	0.16	0.11	0.10
K	1.75	1.75	1.80	1.58	1.61	3.89	3.78	3.71	3.77
F-	0.16	0.13	0.19	0.14	–	–	–	–	–
Total	14.02	13.98	14.05	13.74	13.70	19.95	19.95	19.86	19.90

All oxides are reported as wt% and all cations are reported as atoms per formula unit (apfu) based on 22 oxygen atoms for muscovite and 32 for adularia. In case of cation deficiency in the octahedral site Al is added to Si to achieve full occupancy; Sn, Mn, and Cl were measured, but were always below detection limit

n.d. not detected, *n.a.* not analysed

metal stage of Cordilleran polymetallic vein formation at Morococha. Monazite can be distinguished by its high relief, high birefringence colours of 2nd-3rd order, and a typical euhedral crystal shape ranging from small prisms to near equilateral rectangles (Fig. 7d). Well-formed equilateral monazites are found in clusters of 4–7 or more crystals (Fig. 7h, i), which is reported to be a characteristic feature of hydrothermal monazites (Schandl and Gorton 2004). Monazite from sample KMO-7-241 (Veta Jackeline in Sulfurosa) always occurs together with muscovite in irregular veinlets with tennantite-sphalerite cores cutting quartz vein gangue (Fig. 7f, g). Petrographic evidence for intergrowth indicates equilibrium conditions for both minerals (Fig. 7g). Both monazite and muscovite were separated from the same sample and dated for comparison. Adularia (KMO-6-273; KMO-6-100) was sampled from the late carbonate stage of Cordilleran polymetallic veins. Sample KMO-6-273 is a quartz-rich 2 cm-thick sphalerite- and pyrite-bearing vein with a sericitic alteration halo cutting the altered Codiciada microdiorite in the Codiciada open pit. During a later mineralising phase (i.e. carbonate stage), the vein was reopened and a thin white carbonate vein (~2 mm) was deposited (Fig. 8e). Together with the carbonate, smaller amounts of fine-grained adularia and chlorite were deposited (Fig. 8f), and they represent the last phase of polymetallic mineralisation at Morococha. A greenish chlorite halo of 3 mm borders the vein and overprints the sericitic halo, and it gradually loses intensity further away from the vein (Fig. 8e). Adularia extracted from all of the samples are nearly pure K-feldspar with a low Na_2O content (~0.1–0.4 wt%) and low BaO content (~0.2–0.3 wt%). Representative electron microprobe analyses are reported in Table 3. The paragenetic position of the dated minerals within the evolution of the Cordilleran polymetallic veins is shown in the generalised paragenetic sequence in Fig. 6.

Geochronology results

U-Pb geochronology

Five monazite fractions from one sample (KMO-7-241) were analysed including one single grain (mz 1) and multi-grain fractions of 3 to 8 grains each (mz 2, 3, 4, and 6). All five hydrothermal monazite fractions are analytically concordant and yield a weighted mean $^{206}Pb/^{238}U$ age of 8.26±0.18 Ma (Fig. 9). Uranium content varies between 720 and 3810 ppm, and Th to U ratios are low and range between 0.5 and 1.6 (Table 4). Low Th contents are in agreement with typically low values of this element reported for other hydrothermal monazites, whereas magmatic monazite normally contains at least 1–2 wt% Th (Schandl and Gorton 2004).

Four single hydrothermal titanite crystals (KMO-6-236) yield concordant results and a weighted mean $^{206}Pb/^{238}U$ age of 9.3±0.2 Ma. Uranium content is low at 180–300 ppm, and Th/U ratio shows a very small variation between 2.1 and 3.1 (Fig. 10, Table 4).

$^{206}Pb/^{238}U$ age calculations from these data are more precise than the $^{207}Pb/^{235}U$ age, but they are very sensitive to the choice of common Pb isotope composition due to the relatively low radiogenic Pb/common Pb (Pb*/Pbc) ratios in both monazite (0.7–0.2) and titanite (0.6–0.2). In general, the correction used for initial isotopic composition of lead can be chosen using several methods: (a) using the Pb isotope composition of a co-genetic, low U mineral; (b) using the Pb evolution model of Stacey and Kramers (1975), or (c) employing 3D isochron regression techniques. Since Pb isotopic data from co-genetic low U minerals from the same rock sample is not available, the $^{206}Pb/^{204}Pb$ and $^{207}Pb/^{204}Pb$ values for common Pb in titanite and monazite were calculated using the Pb growth model of Stacey and Kramers (1975), and a total 3D Pb-U isochron solution. Calculated $^{206}Pb/^{204}Pb$ and $^{207}Pb/^{204}Pb$ ratios of the common lead composition using the Pb growth model and a 3D isochron overlap within their uncertainties. Applying these different methods for the common lead correction yields mean $^{206}Pb/^{238}U$ dates for monazite ranging from 8.26±0.18 to 7.9±0.6 Ma (methods 2 and 3, respectively), and for titanite ranging from 9.3±0.2 to 9.32±0.13 Ma (method 2 and 3, respectively). We conclude that the chosen method of correction of the common lead does not influence the accuracy of the $^{206}Pb/^{238}U$ dates, and we report our data corrected with the Stacey and Kramers (1975) model.

Another possible source of inaccuracy on the calculated $^{206}Pb/^{238}U$ dates is the correction for ^{230}Th disequilibrium during crystal growth (Schärer 1984). Correcting the $^{206}Pb/^{238}U$ dates for excess ^{206}Pb requires knowledge of the Th/U of the melt/fluid from which the minerals crystallised. The effect of different $Th/U_{melt/fluid}$ on $^{206}Pb/^{238}U$ dates was tested by applying two extreme values of Th/U of the melt/fluid (i.e. 0.5 and 8) and comparing them with uncorrected $^{206}Pb/^{238}U$ dates. For monazite, the difference between uncorrected $^{206}Pb/^{238}U$ dates and those corrected with $Th/U_{melt/fluid}=0.5$ and 8 is 0.13 and 0.11 Ma. For titanite the difference is 0.28 and 0.07 Ma, respectively. Since the variation in $^{206}Pb/^{238}U$ date remains within the analytical uncertainty (0.18 Ma for monazite and 0.2 Ma for titanite), we prefer not to apply these corrections, because no proxy for estimation of the Th/U ratio of the hydrothermal fluid is available.

Re-Os geochronology

Re-Os data are reported at two-sigma uncertainty (Table 5). The molybdenite age is calculated using $^{187}Os=^{187}Re\ (e^{\lambda t}-1)$ and includes propagated analytical errors and the ^{187}Re decay constant uncertainty. The ^{187}Re decay constant used is 1.666×10^{-11} $year^{-1}$ (Smoliar et al. 1996). The Re concentration for molybdenite from sample KMO-7-407 is 189 ppm. A small amount of common Os (1.311±0.002 ppb) was detected and this is almost certainly derived from small amounts of pyrite, which were unavoidably incorporated during drilling of the molybdenite grains. The amount of radiogenic Os (18.33±0.01 ppb) is 14 times greater than the common Os. Use of the double Os spike allows correction for this common Os, but an initial ratio must be assumed in the calculation. Still, the common Os is low enough that the assumed initial ratio does not affect the calculated age. For example, if the initial $^{187}Os/^{188}Os$ ratio is 0.2, the age is 9.26±0.03 Ma (Table 5); if the initial ratio is increased to 1.0, the age decreases slightly to 9.19±0.03 Ma. In either case, the age overlaps with the U-Pb hydrothermal titanite age of 9.3±0.2 Ma for Codiciada skarn.

Re-Os analyses of Morococha pyrites (KMO-7-244 and KMO-6-102) with high $^{187}Re/^{188}Os$ reveal that both pyrites have significant common Os, comprising more than half of the total Os. This, combined with their low Re concentrations and their very young geological age, precludes any meaningful age calculation. The pyrite from Sulfurosa (KMO-7-244), however, has a high $^{187}Os/^{188}Os$, and the fluid that deposited this pyrite must have been carrying very radiogenic Os.

$^{40}Ar/^{39}Ar$ geochronology

Eight weighted mean $^{40}Ar/^{39}Ar$ ages and one total fusion age are presented in Table 6 and Fig. 10. All plateau ages overlap with their corresponding inverse isochron ages (Fig. 10). Eight of nine samples have inverse isochron $^{40}Ar/^{36}Ar$ intercepts equal to atmospheric argon. All of the ages discussed

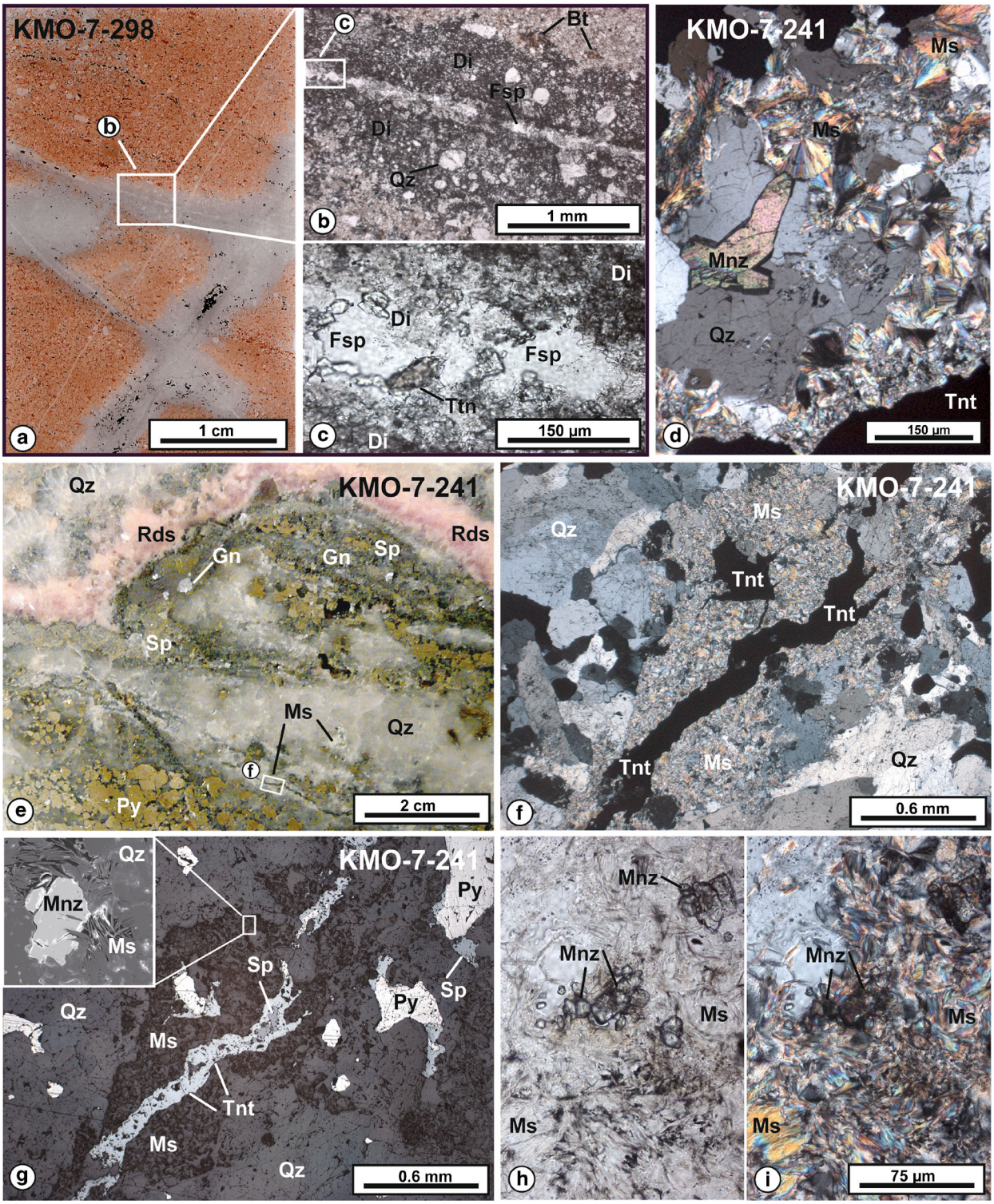

Fig. 7 Photographs of rock slabs and thin section photomicrographs of samples used for dating. **a** Thin section scan of biotite-rich rock (*reddish-brown*) cross-cut by small veinlets that alter the biotite to diopside (*grey*). **b** The veins consist of albite, diopside, and minor titanite (**c**). **d** Monazite and muscovite grains in quartz vein gangue of Cordilleran polymetallic vein sample KMO-7-241 (**e**). **e** Polished slab of Cordilleran polymetallic vein indicating position of (**f**). **f** Photomicrograph of tennantite-muscovite veinlet cross-cutting quartz in crossed-polarised transmitted light; **g** same as (**f**) in reflected light. Cores of the veinlets consist of sphalerite and tennantite. The muscovite dominated halos are clearly visible by their *darker colour*; a secondary electron SEM image in the left upper corner shows monazite intergrown with muscovite flakes; **i** photomicrograph of clustered monazite crystals in muscovite in plane-polarised transmitted light; **h** same as (**i**) in crossed-polarised transmitted light. Abbreviations: *Bt* biotite, *Cal* calcite, *Chl* chlorite, *Fsp* feldspar, *Di* diopside, *Gn* galena, *Ms* muscovite, *Mnz* monazite, *Py* pyrite, *Qz* quartz, *Rds* rhodochrosite, *Sp* sphalerite, *Ttn* titanite, *Tnt* tennantite, *Tr* tremolite

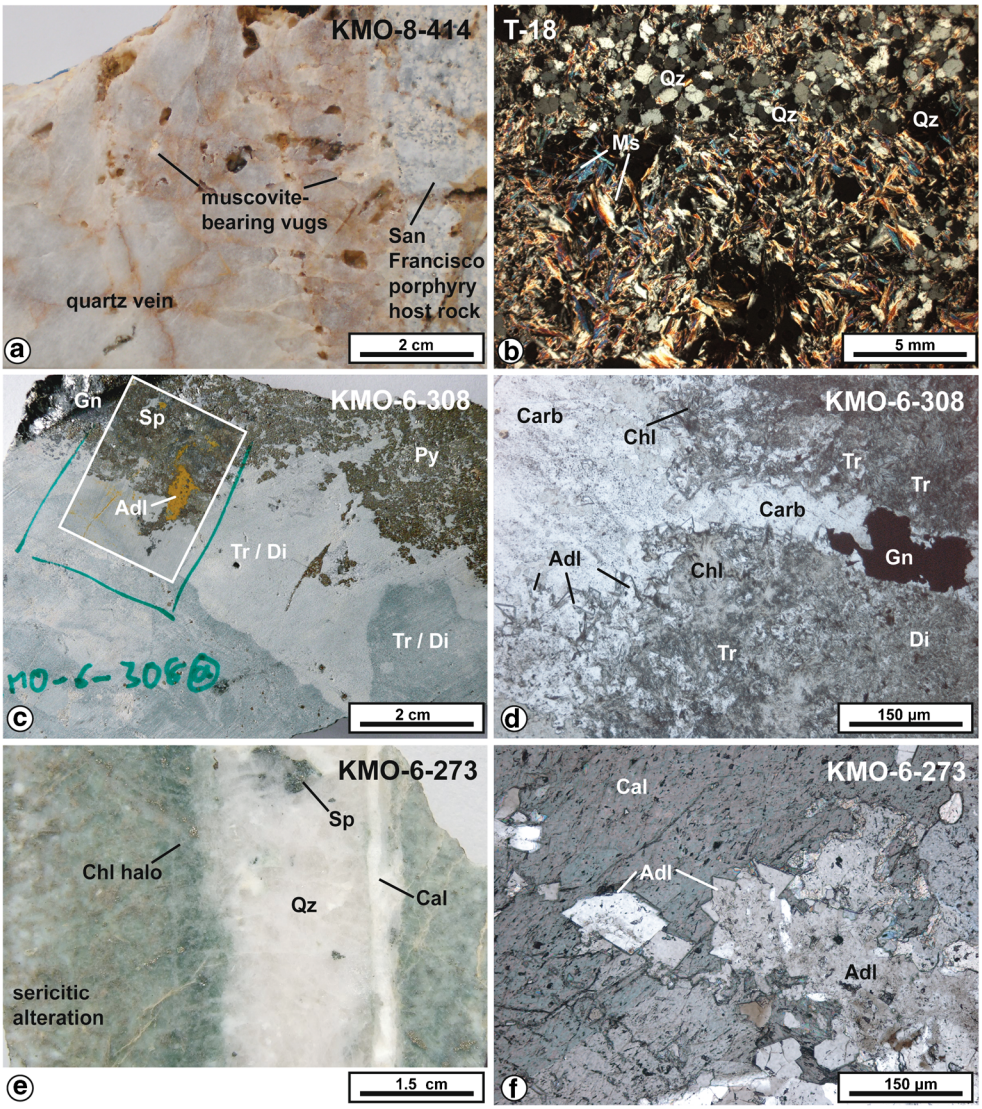

Fig. 8 Photographs of rock slabs and thin section photomicrographs of samples used for dating. **a** Massive porphyry-type quartz vein with sericitic alteration of the host rock. Muscovite is found in small vugs within the vein. **b** Photomicrograph, in crossed-polarised transmitted light, of the Ticlio porphyry rock showing strong sericitic alteration; all feldspars are completely altered to coarse-grained muscovite. **c** Polished slab of fine-grained diopside-tremolite skarn (Manto Italia) showing adularia intergrown with sulphides; *box: orange patches* indicate etched and coloured adularia. **d** Photomicrograph, in plane-polarised transmitted light, of carbonate-galena-adularia veinlet cross-cutting skarn mineral assemblages. **e** Polished slab of Cordilleran polymetallic vein with sericitic outer and chloritic inner halo; a carbonate-adularia vein reopens the quartz-pyrite-sphalerite vein. **f** Photomicrograph, in crossed-polarised transmitted light, of idiomorphic adularia in a matrix of calcite. Abbreviations: *Adl* adularia, *Cal* calcite, *Carb* carbonate, *Chl* chlorite, *Di* diopside, *Gn* galena, *Py* pyrite, *Qz* quartz, *Rds* rhodochrosite, *Sp* sphalerite, *Tr* tremolite

below are weighted mean plateau ages, unless otherwise indicated.

Muscovite from the Ticlio porphyry-type sericitic alteration yields an age of 8.04±0.14 Ma. A younger age of 6.74±0.13 Ma was obtained from muscovite from the porphyry-type quartz-pyrite-molybdenite vein hosted by the San Francisco porphyry stock (KMO-8-203). Muscovite from the porphyry-type milky quartz vein (KMO-8-414) yields a significantly younger age of 5.72±0.18 Ma.

Adularia samples from the Manto Italia polymetallic replacement bodies yield analytically indistinguishable ages of 6.0±0.2 (KMO-6-306) and 6.23±0.12 Ma (KMO-6-308). Adularia from the quartz-rich polymetallic vein (KMO-6-273) gives an age of 5.78±0.10 Ma which is within error of the $^{40}Ar/^{39}Ar$ age obtained from the adularia extracted from sample KMO-6-306. Adularia KMO-6-308 yields a $^{40}Ar/^{36}Ar$ intercept value of 340±40 in inverse isochron space, which is slightly above the atmospheric value (295.5), and indicates that excess ^{40}Ar is

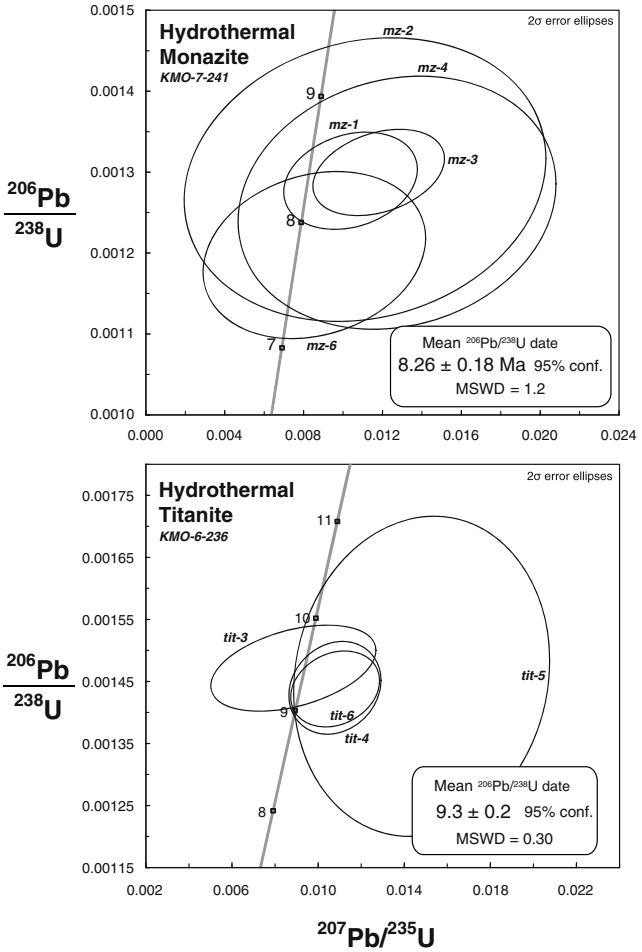

Fig. 9 U-Pb concordia diagrams: **a** hydrothermal monazite from Cordilleran vein gangue and **b** hydrothermal titanite from Na-Ca alteration of the Codiciada microdiorite. Weighted mean dates are reported in 95 % confidence level

present. Therefore, the age may be slightly overestimated, accounting for its higher mean age relative to sample KMO-6-306. However, the uncertainties of the individual steps within this age plateau overlap, and don't reveal the classic topological presence of excess ^{40}Ar within the age spectrum. Removing the first, lowest temperature step out of the plateau would yield a slightly younger plateau age of 6.20± 0.11 Ma and reduce the ^{40}Ar/^{36}Ar intercept value so it overlaps with an atmospheric composition. The two ages are indistinguishable within error and thus the older and more reliable age is used for discussion.

The step-heating analysis of muscovite KMO-7-241 yielded a disturbed age spectrum with no plateau and a total fusion age of 8.1±0.5 Ma. Adularia sample KMO-6-100 gives an age spectrum with high initial ages at low temperature steps that decrease with increasing ^{39}Ar released, and corroborate the presence of excess ^{40}Ar during early degassing, as shown in the inverse isochron plot (Fig. 10). Three higher temperature steps yield indistinguishable ages with a weighted mean age of 7.6±0.3 Ma, although they only account for 44.1 % of the total ^{39}Ar released, and hence not conform to the plateau definition employed here (Dalrymple and Lanphere 1971). Detailed step-heating results are presented in ESM 2.

Discussion

The Morococha district is characterised by a multitude of localised magmatic and hydrothermal events. The age data for hydrothermal events obtained in this study span over 3.4 Ma, from 9.3 to 5.7 Ma. Large porphyry Cu deposits, like Chuquicamata, El Teniente, or Bajo de la Alumbrera and other Andean deposits, are long-lived porphyry-centred districts and formed over several million years (Ballard et al. 2001; Barra et al. 2013; Deckart et al. 2014; Harris et al. 2008; Maksaev et al. 2004; Sillitoe 2010; Sillitoe and Mortensen 2010; Zimmerman et al. 2008). Districts like these consist of large magmatic-hydrothermal complexes that were built during successive magmatic-hydrothermal events triggered by episodic magmatic activity with significant time gaps (Ballard et al. 2001; Sillitoe and Mortensen 2010; Simmons et al. 2013).

Based on our data and previously published age data of magmatic and hydrothermal systems (Bendezú 2014, personal communication; Bendezú et al. 2012; Beuchat 2003; Catchpole 2011; Eyzaguirre et al. 1975; Kouzmanov et al. 2008), we can resolve three individual magmatic-hydrothermal centres at Morococha (Figs. 11 and 12).

Codiciada centre

The Codiciada centre encompasses several magmatic intrusive and hydrothermal mineralising events, which all occurred within a restricted area of about 1 km^2 and are roughly outlined by the Codiciada composite stock (Fig. 12). The Re-Os age (9.26± 0.03 Ma) of molybdenite from Codiciada porphyry-type quartz-molybdenite veins overlaps with the magmatic ages of Codiciada porphyry intrusions at 9.30±0.03 Ma and 9.29± 0.01 Ma, as do the titanite U-Pb age of 9.3±0.2 Ma from the Na-Ca-alteration and anhydrous skarn formation and the ^{40}Ar/^{39}Ar cooling age of 9.5±0.2 Ma for K-feldspar from an aplitic dyke (Bendezú 2014, personal communication; Bendezú et al. 2012). The Na-Ca-alteration pervasively overprints the Codiciada microdiorite and aplitic dyke. A younger cooling age was obtained for hydrous skarn formation, dated by ^{40}Ar/^{39}Ar (phlogopite) at 8.81±0.18 Ma (Kouzmanov et al. 2008). This age post-dates anhydrous skarn and porphyry mineralisation, as well as the ^{40}Ar/^{39}Ar cooling age of K-feldspar from the aplitic dyke, by approximately 0.5 Ma.

Located several kilometres to the southwest of the Codiciada centre, the San Francisco porphyry intrusion has U-Pb ages of 9.11±0.10 and 9.42±0.17 Ma, which are comparable with the Codiciada intrusive ages within analytical uncertainty (Bendezú et al. 2012; Beuchat 2003).

Table 4 Results of U-Pb dating of hydrothermal monazite and titanite

	Compositional parameters				Radiogenic isotope ratios										Corr.	Isotopic ages					
Sample	Weight [mg]	U [ppm]	Th/U	Pb ppm	$\frac{Pb^*}{Pb_c}$	Pb_c [pg]	$\frac{^{206}Pb}{^{204}Pb}$	$\frac{^{208}Pb}{^{206}Pb}$	$\frac{^{207}Pb}{^{206}Pb}$	% err	$\frac{^{207}Pb}{^{235}U}$	% err	$\frac{^{206}Pb}{^{238}U}$	% err	coef.	$\frac{^{207}Pb}{^{206}Pb}$	±	$\frac{^{207}Pb}{^{235}U}$	±	$\frac{^{206}Pb}{^{238}U}$	±
(a)	(b)	(c)	(d)	(c)	(e)	(e)	(f)	(g)	(g)	(h)	(g)	(h)	(g)	(h)		(i)	(h)	(i)	(h)	(i)	(h)
KMO-7-241 hydrothermal monazite, Veta Jackeline, Sulfurosa																KMO-7-241 hydrothermal monazite, Veta Jackeline, Sulfurosa					
mz-1	0.0018	723	0.53	21	0.05	36.09	22	0.2142	0.05839	26.06	0.010379	26.70	0.001289	3.81	0.24	544.24	568.64	10.48	2.78	8.31	0.31
mz-2	0.0006	1317	0.98	35	0.07	19.75	22	0.4467	0.06590	22.24	0.011808	23.09	0.001300	3.35	0.32	803.16	466.64	11.92	2.74	8.37	0.28
mz-3	0.0010	3808	0.74	279	0.02	272.96	20	0.3761	0.07321	51.20	0.012740	51.71	0.001262	10.12	0.15	1019.67	1037.44	12.85	6.60	8.13	0.82
mz-4	0.0010	3407	1.60	284	0.02	276.99	20	0.6832	0.06247	66.66	0.011118	67.41	0.001291	11.09	0.15	690.35	1429.33	11.23	7.53	8.32	0.94
mz-6	0.0010	3483	1.12	168	0.03	162.81	20	0.4021	0.05175	52.99	0.008544	53.96	0.001198	7.04	0.20	274.31	1215.93	8.64	4.64	7.72	0.54
KMO-6-236 hydrothermal titanite (skarn / Ca-Na alteration), Codiciada																KMO-6-236 hydrothermal titanite (skarn/Ca-Na alteration), Codiciada					
tit-3	0.0031	303	3.06	5	0.16	14.58	25	0.9237	0.04362	34.02	0.008850	35.43	0.001471	3.85	0.41	132.06	843.12	8.95	3.16	9.48	0.37
tit-4	0.0082	251	2.29	4	0.19	26.08	26	0.8623	0.05443	15.26	0.010790	15.63	0.001438	3.48	0.22	388.74	343.23	10.90	1.69	9.26	0.32
tit-5	0.0079	178	2.08	9	0.06	68.15	21	1.0525	0.07364	34.55	0.014808	32.80	0.001458	14.46	0.10	1031.71	699.84	14.93	4.86	9.39	1.37
tit-6	0.0113	228	2.86	4	0.18	38.08	25	1.0690	0.05431	16.06	0.010781	16.21	0.001440	4.24	0.16	383.86	362.09	10.89	1.76	9.27	0.40

(a) "mz-" and "tit-" are labels for fractions composed of 2 to 8 monazite and titanite grains or fragments, respectively, except mz-1 which is one grain

(b) Nominal fraction weights measured

(c) Nominal U and total Pb concentrations subject to uncertainty in weighting

(d) Model Th/U ratio calculated from radiogenic $^{208}Pb/^{206}Pb$ ratio and $^{207}Pb/^{235}U$ age

(e) Pb* and Pbc represent radiogenic and common Pb, respectively

(f) Measured ratio corrected for spike and fractionation only. Mass fractionation correction of 0.13±0.02 (1-sigma)%/amu (atomic mass unit) for Pb was applied to all single-collector SEM analyses, based on analysis of NBS-981 and NBS-982. Uranium mass fractionation is corrected in real-time using the $^{233}U/^{235}U$ ratio of the double spike solution

(g) Corrected for fractionation, spike, and common Pb; up to 1.8 pg (monazite) and up to 5 pg (titanite) common Pb was assumed to be procedural blank: $^{206}Pb/^{204}Pb$=18.30±0.71 %, $^{207}Pb/^{204}Pb$=15.47 ±1.03 %, and $^{208}Pb/^{204}Pb$=37.60±0.78 % (all uncertainties 1-sigma). The excess over blank was assigned to initial common Pb at 9 Ma (Stacey and Kramers 1975)

(h) Errors are 2-sigma, propagated using the algorithms of Schmitz and Schoene (2007)

(i) Calculations are based on the decay constants of Jaffey et al. (1971). $^{206}Pb/^{238}U$ and $^{207}Pb/^{206}Pb$ ages are not corrected for initial disequilibrium in $^{230}Th/^{238}U$

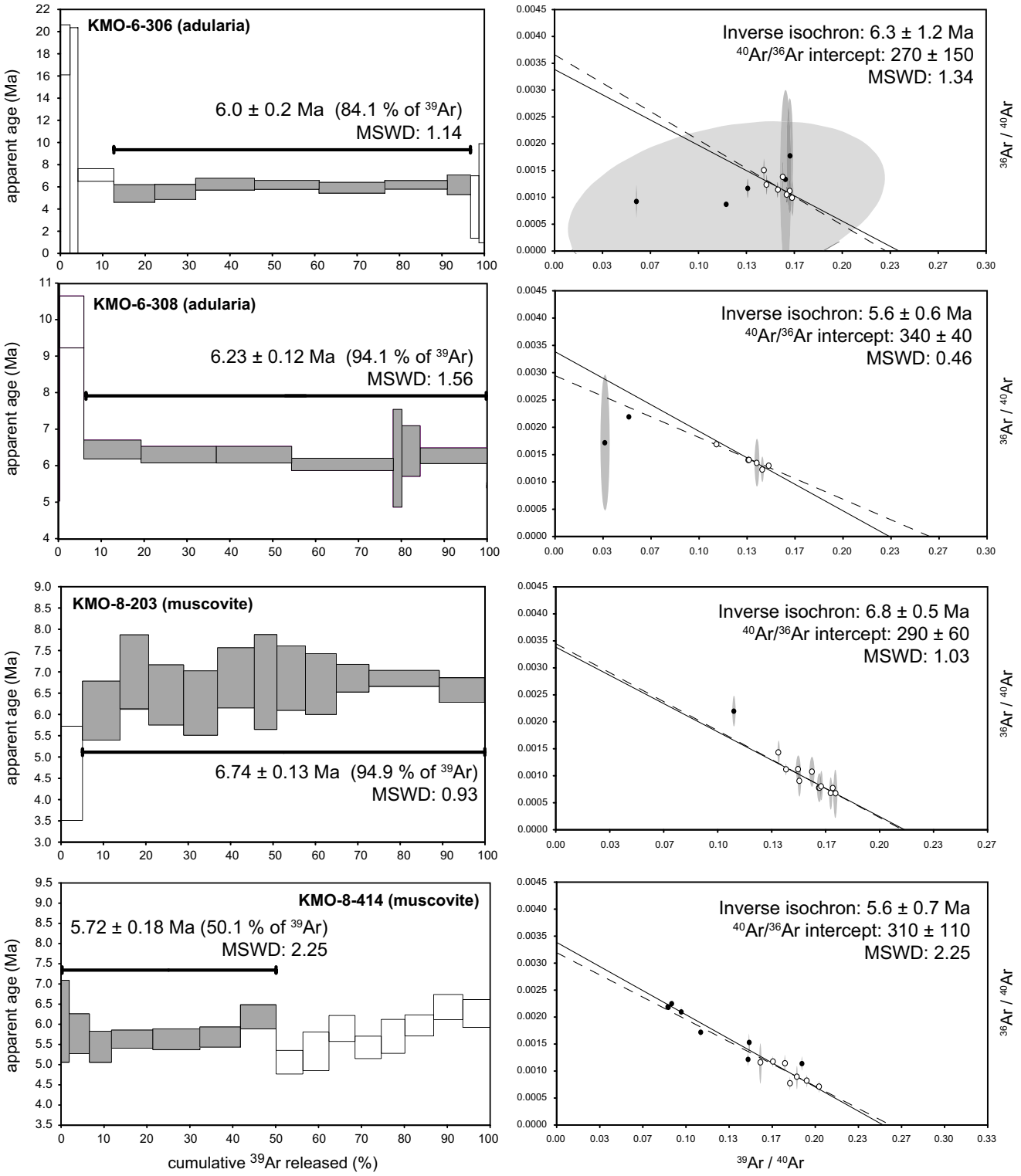

Fig. 10 *Left column* $^{40}Ar/^{39}Ar$ apparent age spectra obtained by step-heating with a CO_2-IR laser. *Grey boxes* indicate those steps that have been used to calculate the plateau ages. Sample KMO-7-241 shows a total fusion age, with no plateau age. *Right column* Inverse isochron correlation diagrams; *solid line* = reference line between the calculated $^{39}Ar/^{40}Ar$ intercept and the inverse atmospheric ratio $^{36}Ar/^{40}Ar$; *dashed line* = least squares regressions plot of the steps included in the plateau; heating steps included in the weighted mean plateau ages are *circles* and the heating steps that are not included are *black dots*

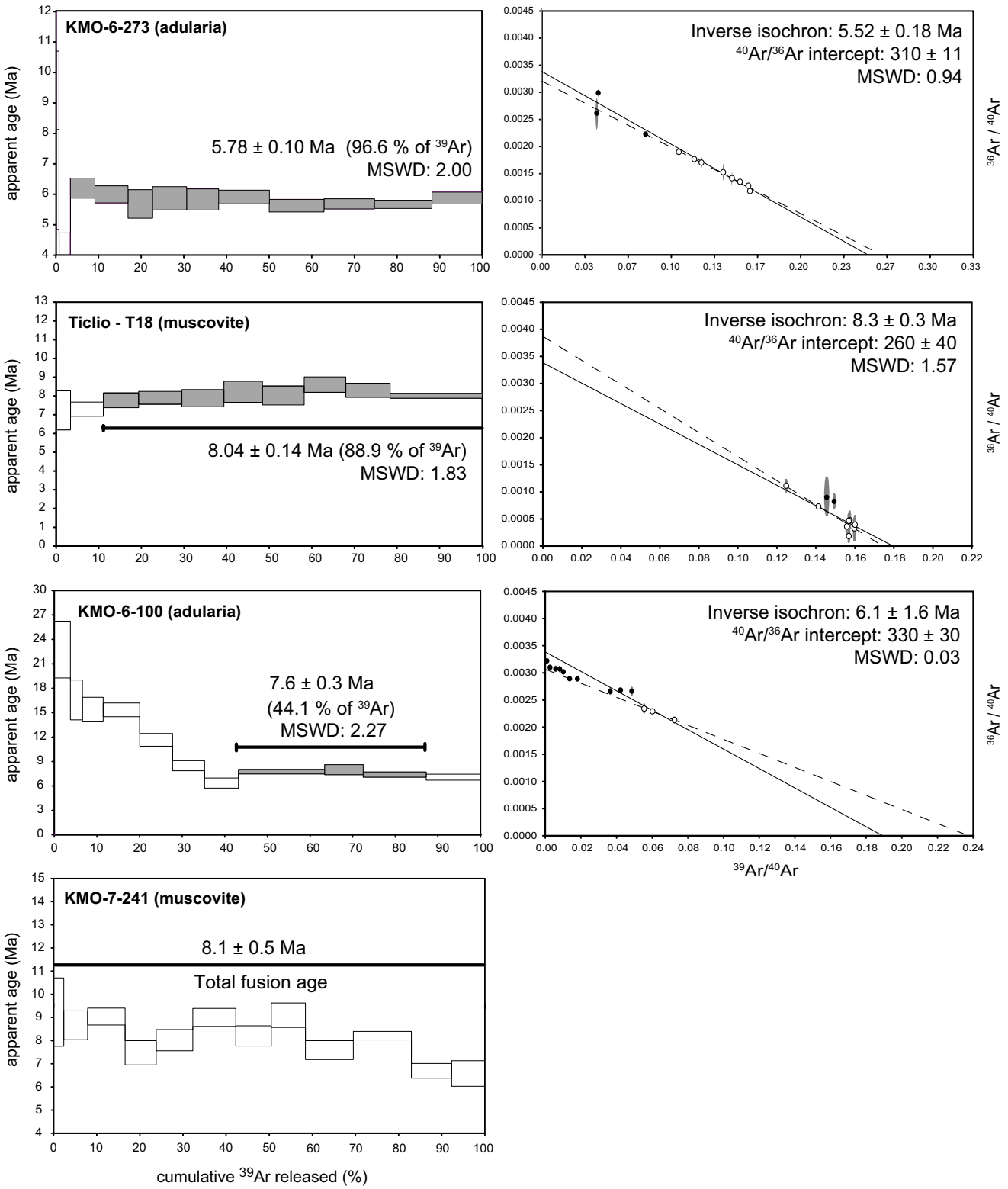

Fig. 10 (continued)

The emplacement of porphyry plugs, formation of porphyry mineralisation and anhydrous skarn, and cooling took place over a relatively short time span of less than 0.2 Ma. This is in agreement with results from other porphyry systems that show how magmatic and hydrothermal events can occur within a very short time frame, and frequently cannot be

Table 5 Re-Os data for molybdenite and pyrite

AIRIE Run #[a]	Sample Name	Mineral	Re, ppm	^{187}Os, ppb	Common Os, ppb	Age, Ma (Os_i=0.2)	Age, Ma (Os_i=1.0)
MD-1159	KMO-6-407, Codiciada (qz-mo vein)	molybdenite	189.0±0.1	18.33±0.01	1.311±0.002	9.26±0.03	9.19±0.03
AIRIE Run #[b]	Sample Name	Mineral	Re, ppb	Total Os, ppb	Common Os, ppb	^{187}Re/^{188}Os	^{187}Os/^{188}Os
LL-549	KMO-7-244, Sulfurosa (massive pyrite body)	pyrite	1.582±0.003	0.0204±0.0009	0.0079	974±2	12.41±0.02
LL-550	KMO-6-102, San Andrés polymetallic vein, Manuelita	pyrite	0.0953±0.0007	0.00281±0.00002	0.0026	178±1	0.813±0.003

[a] Absolute two-sigma uncertainties shown; uncertainty on molybdenite age includes propagated analytical errors and the ^{187}Re decay constant uncertainty; Data are fractionation and blank corrected; common Os is measured and corrected

[b] Data are blank corrected—Re blank=15.64±0.39 pg, total Os=0.721±0.004 pg, ^{187}Os/^{188}Os=0.182±0.002

resolved by high-precision dating techniques (Chiaradia et al. 2013; Seedorff et al. 2005; Stein 2014; von Quadt et al. 2011).

Toromocho centre

The earliest magmatic activity in the Toromocho centre post-dates the porphyry intrusions in the Codiciada centre by 1.1 Ma. A series of five porphyry intrusive events spans at least 1.3 Ma. Emplacement began with the granodiorite porphyry at 8.45±0.05 Ma and ended with intrusion of the dacitic porphyry dyke at 7.26±0.02 Ma (Kouzmanov et al. 2008). The barren Yantac porphyry intruded several km to the south of Toromocho and has a slightly older age of 8.81±0.06 Ma (U-Pb, zircon), and younger biotite (8.4±0.4 and 8.30±0.30 Ma) and K-feldspar ^{40}Ar/^{39}Ar cooling ages (8.01±0.12 Ma) which bracket a minimum cooling time span of 0.8 Ma (Fig. 11, Bendezú et al. 2012; Beuchat 2003). This long cooling history is probably the result of a continuous heat supply from the nearby Toromocho magmatic centre, post-dating the Yantac intrusion by 0.4 Ma.

Multiple hydrothermal events formed porphyry-type and skarn mineralisation in the late stages of Toromocho magmatic activity. The oldest event is documented by molybdenite Re-Os ages of 7.97±0.11 and 7.77±0.11 Ma (Beuchat 2003), corresponding to the initial formation of the Toromocho porphyry Cu-Mo deposit. This mineralising event post-dates all dated porphyries except for the barren dacitic dyke (Fig. 11). The timing does not follow the common observation of porphyry-type Cu-Mo sulphides being introduced concomitant with the first porphyries as described in other multi-phased systems (Schütte et al. 2012; Sillitoe 2010).

Hydrothermal biotite from potassic alteration and biotite-bearing veinlets in the Toromocho area yielded overlapping ages of 7.2±0.3 (K-Ar) and 6.81±0.14 Ma (^{40}Ar/^{39}Ar),

Table 6 Summary of ^{40}Ar/^{39}Ar ages from Morococha

Sample	Location	Mineral	Weighted Plateau age (Ma ±2σ)	% of ^{39}Ar in plateau age	Weighted Plateau age MSWD	Total Fusion age (Ma ±2σ)	Inverse isochron age (Ma ±2σ)	Inverse isochron derived MSDW	Inverse isochron 40/36 ratio of intercept (±2σ)
Quartz-rich porphyry-type vein:									
KMO-8-414	San Francisco	Muscovite	5.72±0.18	50.1	2.25	5.76±0.09	5.6±0.7	2.25	310±110
KMO-8-203	San Francisco	Muscovite	6.74±0.13	94.9	0.93	6.74±0.18	6.8±0.5	1.03	290±60
Porphyry-type phyllic alteration									
T-18	Ticlio	Muscovite	8.04±0.14	88.9	1.83	7.99±0.13	8.3±0.3	1.57	260±40
Manto Italia polymetallic replacement bodies:									
KMO-6-306	Manto Italia	Adularia	6.0±0.2	84.1	1.14	6.4±0.3	6.3±1.2	1.34	270±150
KMO-6-308	Manto Italia	Adularia	6.23±0.12	94.1	1.56	6.49±0.11	5.6±0.6	0.46	340±40
Cordilleran polymetallic vein:									
KMO-6-273	Codiciada	Adularia	5.78±0.10	96.6	2.00	5.77±0.08	5.52±0.18	0.94	310±11
KMO-6-100	Manuelita	Adularia	**7.6±0.3**	44.1	2.27	10.0±0.2	6.1±1.6	0.03	330±30
KMO-7-241	Sulfurosa	Muscovite	–	–	–	8.1±0.5	–	–	–

Plateau ages calculated according to the criteria of Dalrymple and Lanphere (1971); the age set in bold is calculated on the basis of <50 % total released ^{39}Ar

MSWD mean square of weighted deviates

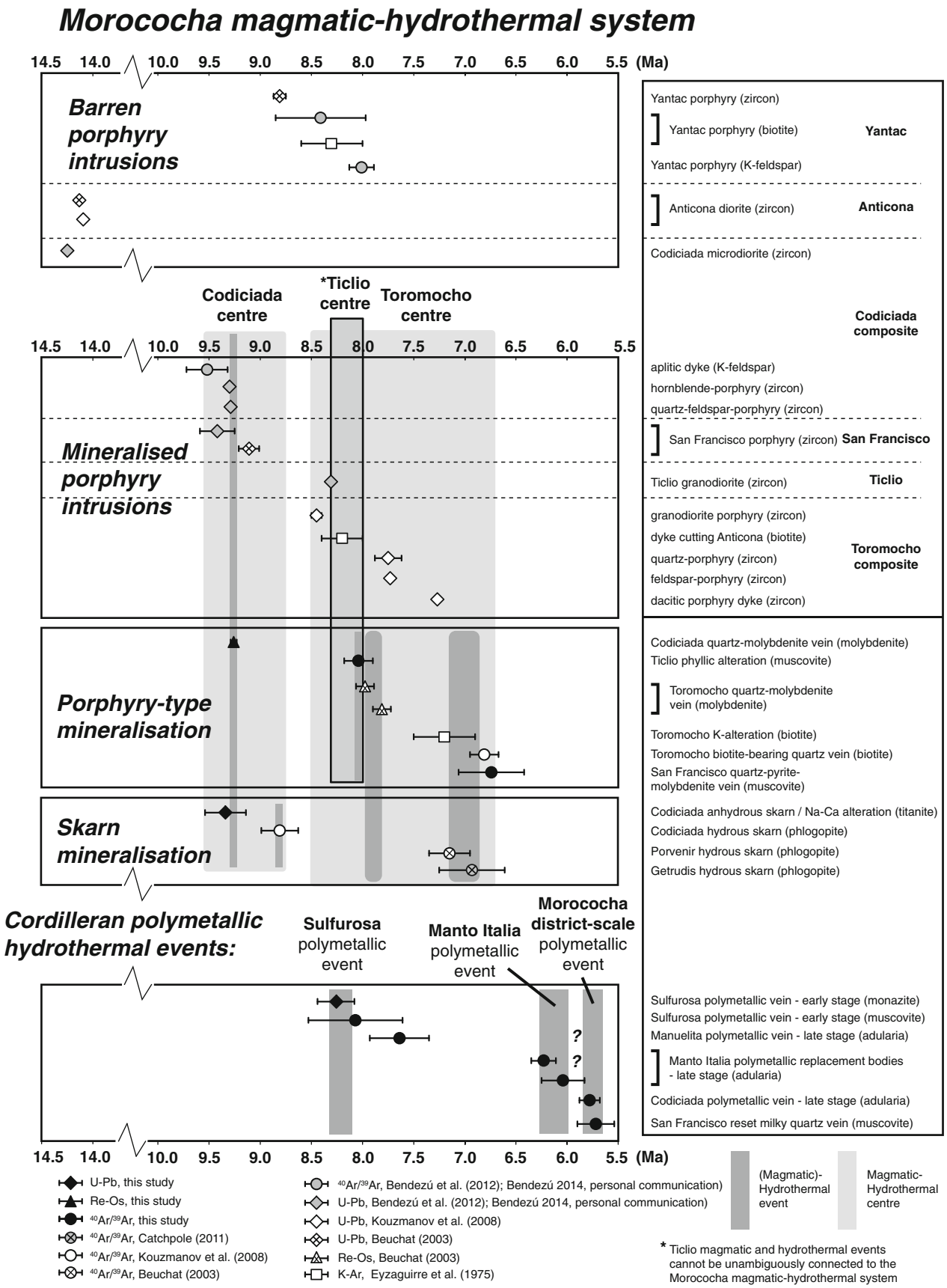

Fig. 11 Summary diagram for the timing of middle to late Miocene magmatic and hydrothermal events of the Morococha magmatic-hydrothermal system

respectively (Eyzaguirre et al. 1975; Kouzmanov et al. 2008). According to field observations, the potassic alteration and biotite-bearing veins are cross-cut by quartz-molybdenite veins that are at least 0.6 Ma older (8.0–7.8 Ma, Re-Os; Beuchat 2003). Therefore, the ages of the hydrothermal biotite are interpreted to be reset cooling ages and to represent a thermal or hydrothermal event that post-dates the original biotite formation. In total, five K-bearing minerals yield overlapping $^{40}Ar/^{39}Ar$ cooling ages between 7.2 and 6.8 Ma (Fig. 11). Muscovite from the quartz-pyrite-molybdenite vein hosted by the San Francisco porphyry intrusion has a cooling age of 6.74±0.13 Ma and is in good agreement with the phlogopite cooling age of 6.9±0.3 Ma for the Gertrudis skarn (Catchpole 2011) and the Porvenir skarn phlogopite cooling age of 7.2±0.2 Ma (Beuchat 2003). Given the close spatial association with Toromocho, the 6.7 Ma muscovite age from the San Francisco porphyry is likely to have been reset by the same event as the biotite ages at ~7.2–6.8 Ma.

The cooling ages at ~7.2–6.8 Ma demonstrate the minimum size of the Toromocho late hydrothermal activity extending over 6 km^2 (Fig. 12), which is probably responsible for the majority of hydrous skarn formation in central Morococha (Catchpole 2011; Kouzmanov et al. 2008; Lowell and Alvarez 2005). The overlapping ages mark the end of the slowly cooling and long-lived Toromocho magmatic-hydrothermal centre soon after last magmatic activity at 7.26 ±0.02 Ma.

The long-lived magmatic activity such as seen at the Toromocho centre appears to be crucial to the formation of a Cu-Mo deposit of significant size (e.g. Barra et al. 2013; Caricchi et al. 2014; Sillitoe and Mortensen 2010), compared to the relatively short (0.2–0.3 Ma) magmatic-hydrothermal events or "pulses" of the Codiciada and Ticlio centres (see below) that do not yield important amounts of porphyry Cu-Mo or Cu-Au mineralisation.

Ticlio centre

The small Ticlio magmatic-hydrothermal centre was identified and described by Bendezú et al. (2008a). It coincides in time with the first magmatic event in the Toromocho centre. Ticlio is considered an individual centre because it is located ~5 km to the west of Toromocho. Muscovite from the sericitic alteration zone gives a $^{40}Ar/^{39}Ar$ cooling age of 8.04± 0.14 Ma that post-dates the Ticlio porphyry intrusion (8.31± 0.03 Ma, U-Pb zircon age) by approximately 0.3 Ma. The proximity in time between the magmatic and hydrothermal events shows that the Ticlio centre might have been produced by one single magmatic-hydrothermal pulse.

Cordilleran polymetallic hydrothermal events

Three hydrothermal Cordilleran polymetallic events have been identified: the (a) discrete Sulfurosa event, the (b) Manto

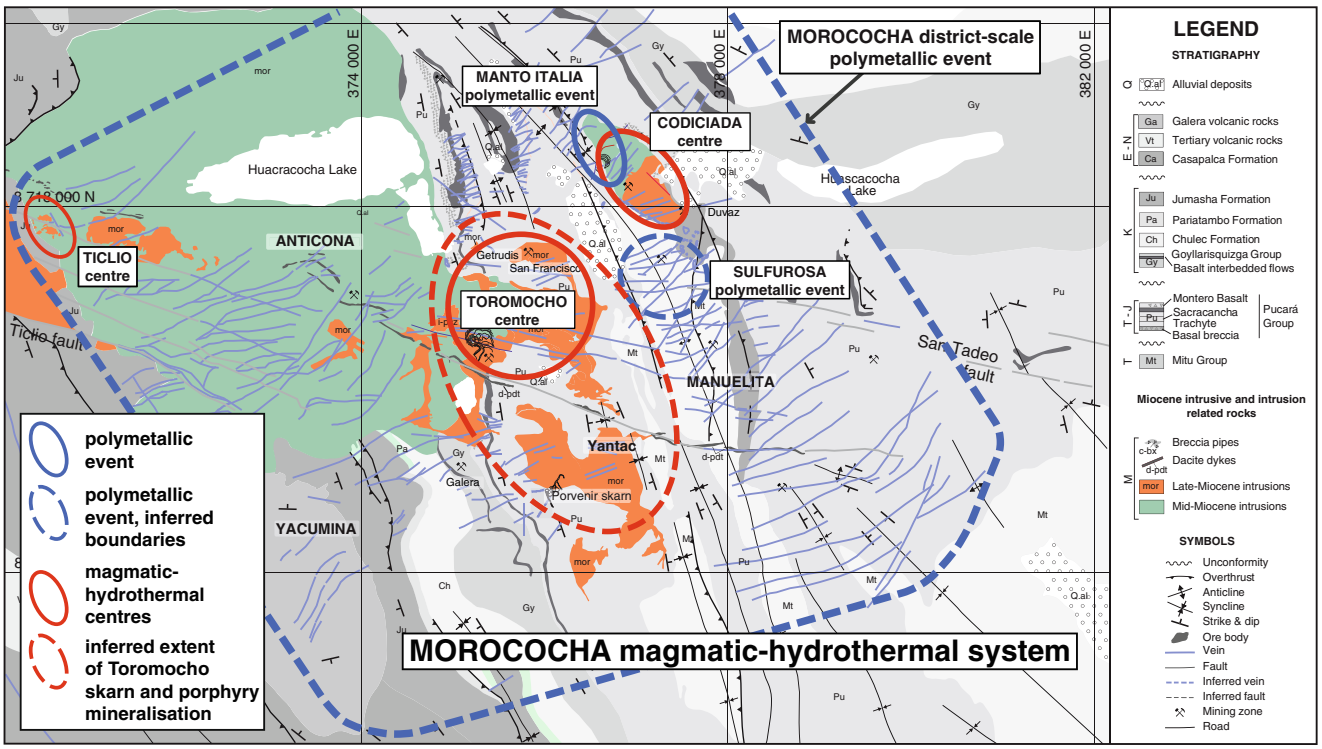

Fig. 12 Summary of all magmatic-hydrothermal centres (*red outlines*) and polymetallic events (*blue outlines*) in the Morococha magmatic-hydrothermal system. All outlines cover the minimum area of mineralisation identified for any individual hydrothermal event. The areas with a dashed outline show inferred event boundaries

Italia event, and (c) the prominent Morococha district-scale polymetallic event.

U-Pb dating of hydrothermal monazites at 8.26±0.18 Ma characterises the discrete Sulfurosa hydrothermal event. The monazites precipitated during the early stages of Cordilleran polymetallic vein formation in the Sulfurosa area. Muscovite from the same vein sample in the same paragenetic position has a disturbed age spectrum and a total fusion $^{40}Ar/^{39}Ar$ age of 8.1±0.5 Ma, which overlaps with the monazite age. It is likely that the Ar isotope systematics were disturbed during one of the later hydrothermal fluid pulses that introduced the base metal mineralisation (see below). The U-Pb monazite age is considered to be more robust than the mica $^{40}Ar/^{39}Ar$ age because the closure temperature for Pb in monazite is substantially higher (700–800 °C) compared to 400 °C and 450 °C for muscovite grain sizes of 100 μm (Harrison et al. 2009; Parrish 1990) and thus Pb diffusion in monazite will be insignificant at mesothermal temperatures (Cherniak et al. 2004). A younger $^{40}Ar/^{39}Ar$ age of 7.6±0.3 Ma (weighted plateau age with 44.1 % ^{39}Ar released) is recorded by adularia from the San Andrés vein in Manuelita and shows a disturbed L-shaped age spectrum which is diagnostic of excess ^{40}Ar in the early degassing steps. This age is not a reliable defined age plateau and is excluded from further discussion. The Sulfurosa polymetallic event has similar geologic and petrographic characteristic to the later base metal veins of the Morococha district-scale polymetallic event.

The Morococha district-scale polymetallic event forms Cordilleran polymetallic (Zn-Pb-Ag-Cu) replacement bodies and abundant veins that cross-cut the entire district. The mineralised area covers 50 km^2 (Fig. 12). Adularia from the carbonate stage of a polymetallic vein in the Codiciada area is dated at 5.78±0.10 Ma, which post-dates the older Sulfurosa hydrothermal event (8.3 Ma, U-Pb monazite age) by about 2.5 Ma and the last Toromocho porphyry mineralising event by about 1 Ma. This $^{40}Ar/^{39}Ar$ age is considered to record precipitation of the adularia and is consistent with rapid cooling. It records the last hydrothermal activity in the district, supported by field and petrographic observations. No evidence of subsequent reheating of the system has been found. Muscovite from vugs in the porphyry-type milky quartz vein in the San Francisco area yield a similar age of 5.72±0.18 Ma. The plateau age has been obtained from the lower temperature degassing steps and is indistinguishable from the total fusion age (5.76± 0.09 Ma). This young age may have been produced by thermal resetting or the precipitation of muscovite by evolving hot fluids circulating through reopened fractures in the quartz vein at a later point in time, corresponding to Cordilleran polymetallic vein formation. The latter is supported by sericite flakes found trapped in some fluid inclusions. Fluid inclusion studies of this vein show that several fluid generations consecutively percolated through multiple fractures in the vein, ultimately related to formation of the Cordilleran polymetallic veins (Catchpole et al. 2015). These fluids range from intermediate-density to liquid-rich fluids, with minimum trapping temperatures of ~420 °C and 260 °C, respectively (Catchpole et al. 2011, 2015). We hence interpret the muscovite date to represent the age of Cordilleran polymetallic mineralisation during the Morococha district-scale polymetallic event.

Manto Italia polymetallic event: Adularia $^{40}Ar/^{39}Ar$ ages of the Manto Italia polymetallic replacement bodies are indistinguishable within error and post-date the youngest porphyry-type mineralisation (6.74±0.13 Ma, $^{40}Ar/^{39}Ar$ muscovite) by approximately 0.5 Ma. One $^{40}Ar/^{39}Ar$ age (6.0±0.2 Ma) overlaps with ages obtained for the Cordilleran base metal veins of the Morococha district-scale polymetallic event, while the other age is several hundred thousand years older (6.23±0.12 Ma). This older sample yields small amounts of excess ^{40}Ar, indicating that the actual age might be slightly younger and could also overlap with the ages for the base metal veins. Taking the partly overlapping analytical uncertainties, it appears reasonable to assume that a single hydrothermal pulse was responsible for the formation of the Manto Italia and the Morococha district-scale polymetallic mineralisation.

Timing of base metal mineralisation in porphyry systems

Results for the timing of base metal mineralisation at Morococha show that the bulk of the Zn-Pb-Ag-Cu sulphides precipitated during an independent hydrothermal event that post-dates the formation of Toromocho porphyry-type Cu-Mo mineralisation by 0.5 Ma. Base metal mineralisation has been documented in several long-lived porphyry-centred districts that contain important porphyry Cu deposits (Ballard et al. 2001; Harris et al. 2008; Maksaev et al. 2004; Sillitoe 2010; Sillitoe and Mortensen 2010; Zimmerman et al. 2008). In Butte, Montana (Table 7; Dilles et al. 2003; Lund and Aleinikoff 2005; Lund et al. 2002; Martin et al. 1999; Meyer et al. 1968; Snee et al. 1999; Stein 2005), Main Stage veins, which are very similar to Morococha polymetallic veins, yield $^{40}Ar/^{39}Ar$ cooling ages of 67–63 Ma. Two porphyry centres have multiple pulses of molybdenite mineralisation spanning 1–2 Ma, from 66 to 64 Ma (Dilles et al. 2003). Porphyry Cu-Mo and Cu-rich base metal veins are formed during hydrothermal events in a 3–4 Ma magmatic-hydrothermal history (Houston and Dilles 2013).

Polymetallic and precious metal mineralisation are usually introduced at a late stage, as seen by textural evidence of reopening of porphyry-type veins and the

Table 7 Overview of deposits with published age data for porphyry-related mineralisation styles

Deposit	Magmatic events	Porphyry-style mineralisation	High-sulphidation/ Cordilleran polymetallic	Age relationship	Spatial relationship to porphyry	Interpretation for genetic link	Reference
Lepanto, Philippines	Imbanguila dacite, host rocks: 2.2–1.8 Ma (K-Ar, 4 hornblende ages)	Far Southeast Cu-Au porphyry; K-alteration: 1.3 - 1.4 Ma (K-Ar, 6 biotite and 10 illite ages)	Lepanto Cu-Au: 1.41–0.05 Ma (K-Ar, average of 10 alunite ages); Victoria: Au-(Cu-Zn-Ag) veins: 1.14±0.02 Ma, 1.16±0.02 Ma (K-Ar, illite vein gangue ages)	Lepanto and the Cu-Au porphyry are indistinguishable in age (1.3-1.4 Ma). Victoria is slightly younger (0.15 Ma) than Lepanto, but overlaps with two Lepanto alunite ages. Victoria carbonate veins cross-cut Lepanto enargite veins	Above (Lepanto) and adjacent, <1 km (Victoria)	Genetic link suggested	Arribas et al. 1995; Hedenquist et al. 1998, 2001
Butte, Montana, USA	Butte Quartz Monzonite: 76.3±0.1 Ma (U-Pb, zircon age); Multiple porphyry intrusions: 70–63 Ma (U-Pb, zircon and monazite ages)	Butte Cu-Mo porphyry mineralisation: 66–65 Ma (Re-Os, molybdenite ages)	Butte Main Stage veins: 70 - 64 Ma ($^{40}Ar/^{39}Ar$, 30 white mica ages); 58 Ma (K-Ar, sericite from vein halo ages); 63 - 62.5 Ma ($^{40}Ar/^{39}Ar$, white mica ages)	Reported porphyry intrusion and mineralisation, and Main Stage vein ages overlap within 70 to 64 Ma (following Lund and Aleinikoff 2005). Main stage mineralisation is bracketed between 65 Ma (pre-Main Stage Modoc porphyry intrusion) and 62.5 Ma (following Dilles et al. 2003)	Cross-cutting porphyry	Genetic link suggested	Meyer et al. 1968; Martin et al. 1999; Snee et al. 1999; Lund et al. 2002; Dilles et al. 2003; Lund and Aleinikoff 2005
Rosario, Collahuasi district, Chile	Rosario monzonite porphyry: 34.4±0.3 Ma ($^{40}Ar/^{39}Ar$, biotite cooling age)	Rosario Cu-Mo: 34.5±0.5 Ma ($^{40}Ar/^{39}Ar$, illite age), 33.3±0.2 Ma (Re-Os, molybdenite age)	Rosario Cu-Ag massive sulphide veins: 32.6±0.3 Ma ($^{40}Ar/^{39}Ar$, alunite age)	Overprint of porphyry mineralisation by high-sulphidation Cu-Ag veins ~0.7 Ma later	Cross-cutting porphyry	Genetic link suggested	Masterman et al. 2004
Colquijirca, Peru	Dacitic dome: 12.9 - 12.4 Ma ($^{40}Ar/^{39}Ar$, 3 magmatic biotite ages)	–	Oro Marcapunta Au-(Ag): 11.9 - 11.1 Ma ($^{40}Ar/^{39}Ar$, 7 alunite ages) Smelter and Colquijirca Cordilleran base metal replacement bodies: 10.8–10.6 Ma ($^{40}Ar/^{39}Ar$, 7 alunite ages)	A 1.3 Ma period (11.9 - 10.6 Ma) of magmatic-hydrothermal activity including an early epithermal Au–(Ag) mineralisation event and a later Cordilleran polymetallic event	–	Genetic link to hidden porphyry suggested	Bendezú et al. 2003; Bendezú et al. 2008a, b
Cerro de Pasco, Peru	Porphyry dykes and dome, and lapilli tuff: 15.4–15.2 Ma (U-Pb, 3 zircon ages)	–	Cu-Ag-Au-(Zn-Pb) enargite-pyrite veins and Zn-Pb-(Bi-Ag-Cu) carbonate replacement bodies: 14.5–14.4 Ma ($^{40}Ar/^{39}Ar$, 7 alunite ages)	1 Ma magmatic-hydrothermal activity with sulphide rich Cordilleran mineralisation forming during a period of about 0.1 Ma post-dating magmatic activity	–	Genetic link to hidden porphyry suggested	Baumgartner et al. 2009
Pierina, Peru	–	–	Pierina Au-Ag deposit: 15.0 - 13.9 Ma ($^{40}Ar/^{39}Ar$, 19 alunite ages); Santo Toribio Ag-Pb-Zn-Cu	Alunite ages are mainly overlapping with two clear events at ~15.0 Ma and 14.4 Ma in a ~1 Ma interval.	–	–	Rainbow 2009

Table 7 (continued)

Deposit	Magmatic events	Porphyry-style mineralisation	High-sulphidation/ Cordilleran polymetallic	Age relationship	Spatial relationship to porphyry	Interpretation for genetic link	Reference
			veins: 15.6–14.2 Ma ($^{40}Ar/^{39}Ar$, 4 vein halo sericite ages)	Sericite ages of polymetallic veins from Santo Toribio overlap			
Chuquicamata, Chile	East Porphyry intrusion: 34.6±0.2 Ma; beginning of main mineralisation process with intrusion of the West and Banco porphyries 33.3±0.3 Ma and 33.5±0.2 Ma (U-Pb, zircon ages)	Potassic alteration together with chalcopyrite: 32.9 – 33.8 Ma ($^{40}Ar/^{39}Ar$, 4 K-feldspar ages); later overprinting quartz-pyrite-sericite stage: 31.1±0.3 Ma ($^{40}Ar/^{39}Ar$, sericite age)	–	Introduction of high-sulphidation minerals about 2 Ma after first porphyry-type mineralisation	Overprinting porphyry mineralisation	Genetic link suggested	Reynolds et al. 1998; Ballard et al. 2001; Faunes et al. 2005; Barra et al. 2013

introduction of base metals, or overprinting by later base metals stages, e.g. as documented in Chuquicamata (Faunes et al. 2005; Ossandón et al. 2001) and Escondida (Ojeda 1986; Padilla Garza et al. 2001). The age of porphyry mineralisation is slightly older or indistinguishable from that of polymetallic and precious mineralisation, e.g. the Far Southeast porphyry Cu-Au and the Lepanto and Victoria polymetallic deposits, Philippines (Arribas et al. 1995; Hedenquist et al. 2001) and Rosario (Collahuasi) porphyry Cu-Au deposits which are overprinted by high-sulphidation Cu mineralisation (Masterman et al. 2004; Muntean and Einaudi 2001; Sillitoe et al. 1991). Within a single magmatic-hydrothermal system the duration of magmatic-hydrothermal activity can span between 0.2 and 1.3 Ma (Baumgartner et al. 2009; Bendezú et al. 2003, 2008b; Prendergast et al. 2005; Rainbow 2009). Where data are available, the base metal events are usually the last mineralising event and post-date precious metal epithermal mineralisation (Bendezú et al. 2008b).

These data show that long-lived magmatic-hydrothermal systems include several magmatic-hydrothermal pulses and are characteristic of long-lived hydrothermal activity that can generate porphyry-type and polymetallic mineral deposits.

Conclusions

Magmatic intrusive activity in the Morococha district ranges from 14.3 to 7.3 Ma. Hydrothermal activity is recorded from 9.3 to 5.7 Ma. The combination of cross-cutting relationships and U-Pb, Re-Os, and $^{40}Ar/^{39}Ar$ age data for porphyry-related hydrothermal events reveal that the Morococha magmatic-hydrothermal system comprises three distinct magmatic-hydrothermal centres that formed over several million years: the Codiciada, Toromocho, and the Ticlio centre, each separated in time and space. During the late Miocene, hydrothermal activity at Morococha led to the formation of economic and sub-economic Cu-Mo porphyries, skarn, pyrite bodies, and Cordilleran polymetallic mineralisation over an area of at least 50 km^2. The first dated hydrothermal event in the Codiciada centre is recorded by a titanite U-Pb age of 9.3± 0.2 Ma for Codiciada Na-Ca alteration and diopside skarn, and a molybdenite Re-Os age of 9.26±0.03 Ma for molybdenite-bearing quartz veins cutting Codiciada microdiorite. Both ages are analytically indistinguishable from zircon U-Pb ages of two other porphyry intrusions in the Codiciada composite stock, indicating a time span of porphyry emplacement and skarn and porphyry-type mineralisation of <0.2 Ma. The Ticlio magmatic-

hydrothermal centre has a maximum duration of 0.3 Ma, ranging from porphyry emplacement to porphyry mineralisation at 8.04±0.14 Ma ($^{40}Ar/^{39}Ar$ muscovite cooling age). The ages of porphyry and skarn mineralisation correspond well with the magmatic ages and setting in the Morococha district, for both the Codiciada and the Ticlio centres.

The Toromocho magmatic-hydrothermal centre, with a minimum of five porphyry intrusions, spans 1.3 Ma and is responsible for the formation of the Toromocho Cu-Mo deposit. At least two separate hydrothermal events are recorded, the first one producing molybdenite mineralisation at 8.0–7.8 Ma (7.97±0.11 and 7.77±0.11 Ma; Beuchat 2003), and the second one widespread hydrous skarn and resetting of biotite at 7.2–6.8 Ma (five $^{40}Ar/^{39}Ar$ cooling ages). The overlapping cooling ages cover an area of over 6 km^2 and mark the end of the slowly cooling and long-lived Toromocho magmatic-hydrothermal centre soon after last magmatic activity at 7.26±0.02 Ma.

The formation of district-wide Cordilleran base metal veins (5.78±0.10 and 5.72±0.18 Ma; $^{40}Ar/^{39}Ar$ ages) and the Manto Italia polymetallic replacement bodies (6.23±0.12 and 6.0±0.2 Ma; $^{40}Ar/^{39}Ar$ ages) are interpreted to have resulted from one hydrothermal event that post-dates the youngest recorded porphyry mineralisation by more than 0.5 Ma. Hydrothermal activity ceased after formation of the Cordilleran polymetallic veins.

A separate polymetallic event, the Sulfurosa polymetallic event, is revealed by dating of monazites (U-Pb) and muscovite ($^{40}Ar/^{39}Ar$) from one polymetallic vein, which yield overlapping ages of approximately 8.3 Ma. This event not only predates the major polymetallic event by 2.6 Ma, but also several Toromocho magmatic intrusions and porphyry mineralisation by up to 1.5 Ma. These data show that Cordilleran polymetallic mineralisation can form during individual magmatic-hydrothermal pulses, similar to porphyry- and skarn-type mineralisation, and even pre-date porphyry-type mineralisation. In the field, these events are strongly masked by the Morococha district-wide Cordilleran polymetallic mineralisation, which reopened older mineralised fractures and precipitated a mineral suite which is nearly identical.

This study shows that U-Pb ID-TIMS dating of hydrothermal REE-phosphates from Cordilleran polymetallic veins can produce reliable age data and could prove to be a robust dating tool for other porphyry-related polymetallic mineral deposits when accessory hydrothermal monazite and xenotime are identified.

Acknowledgements This study was supported by the Swiss National Sciences Foundation (Grant 20020-108026), and the Pan American Silver Corp. provided field and logistical support and access to the mine area. Pan American Silver Corp. Morococha staff is gratefully acknowledged for friendly support, Diego Villagómez and Roelant van der Lelij for support during the $^{40}Ar/^{39}Ar$ step heating experiments and discussion of results, and Urs Schaltegger for his support and active participation in the monazite dating process. We thank Thomas Bissig, John Dilles, and Georges Beaudoin for detailed reviews that improved the manuscript and helpful comments by Albert Gilg.

References

Alvarez AA (1999) Yacimiento Toromocho. In: Pro-Explo1999 Lima, Peru. pp 205-225

Arribas AJ, Hedenquist JW, Itaya T, Okada T, Concepción RA, Garcia JSJ (1995) Contemporaneous formation of adjacent porphyry and epithermal Cu-Au deposits over 300 ka in northern Luzon, Philippines. Geology 23:337–340

Ballard JR, Palin JM, Williams IS, Campbell IH, Faunes A (2001) Two ages of porphyry intrusion resolved for the super-giant Chuquicamata copper deposit of northern Chile by ELA-ICP-MS and SHRIMP. Geology 29:383–386

Barra F, Alcota H, Rivera S, Valencia V, Munizaga F, Maksaev V (2013) Timing and formation of porphyry Cu–Mo mineralization in the Chuquicamata district, northern Chile: new constraints from the Toki cluster. Miner Deposita 48:629–651

Bartos PJ (1989) Prograde and retrograde base metal lode deposits and their relationship to underlying porphyry copper deposits. Econ Geol 84:1671–1683

Baumgartner R, Fontboté L, Vennemann T (2008) Mineral zoning and geochemistry of epithermal polymetallic Zn-Pb-Ag-Cu-Bi mineralization at Cerro de Pasco, Peru. Econ Geol 103:493–537

Baumgartner R, Fontbote L, Spikings R, Ovtcharova M, Schaltegger U, Schneider J, Page L, Gutjahr M (2009) Bracketing the age of magmatic-hydrothermal activity at the Cerro de Pasco epithermal polymetallic deposit, central Peru: A U-Pb and $^{40}Ar/^{39}Ar$ study. Econ Geol 104:479–504. doi:10.2113/gsecongeo.104.4.479

Bendezú R, Fontboté L, Cosca M (2003) Relative age of Cordilleran base metal lode and replacement deposits, and high sulfidation Au-(Ag) epithermal mineralization in the Colquijirca mining district, central Peru. Miner Deposita 38:683–694

Bendezú A, Catchpole H, Kouzmanov K, Fontboté L, Astorga C (2008a) Miocene magmatism and related porphyry and polymetallic mineralization in the Morococha district, Central Peru. In: XIII Congreso Latinoamericano de Geología, Lima, Peru, 29 September - 3 Octobre 2008. p 6

Bendezú R, Page L, Spikings R, Pecskay Z, Fontboté L (2008b) New $^{40}Ar/^{39}Ar$ alunite ages from the Colquijirca district, Peru: evidence of a long period of magmatic SO_2 degassing during formation of epithermal Au-Ag and Cordilleran polymetallic ores. Miner Deposita 43:777–789

Bendezú A, Kouzmanov K, Ovtcharova M, Spikings R, Fontboté L (2012) Timing of porphyry emplacement in the Miocene Morococha district, central Peru: U-Pb and Ar-Ar geochronological record. In: 34th International Geological Congress, Brisbane, Australia, 5 – 10th August 2012. p 1

Beuchat S (2003) Geochronological, structural, isotopes and fluid inclusion constraints of the polymetallic Domo de Yauli District, Peru. Terre Environ 41:130

Bissig T, Tosdal RM (2009) Petrogenetic and metallogenetic relationships in the eastern Cordillera Occidental of central Peru. J Geol 117:499–518

Bissig T, Ullrich TD, Tosdal RM, Friedman R, Ebert S (2008) The time-space distribution of Eocene to Miocene magmatism in the central Peruvian polymetallic province and its metallogenetic implications. J S Am Earth Sci 26:16–35

Boggio MS (1980) Morococha. In: Boggio MS (ed) El Peru Minero - Tomo IV: Yacimientos - vol. 1. Lima, Peru, pp 33-42

Bowring JF, McLean NM, Bowring SA (2011) Engineering cyber infrastructure for U-Pb geochronology: Tripoli and U-Pb_Redux. Geochem Geophys Geosyst 12:19. doi:10.1029/2010GC003479

Caricchi L, Simpson G, Schaltegger U (2014) Zircons reveal magma fluxes in the Earth's crust. Nature 511:457–461

Catchpole H (2011) Porphyry-related polymetallic mineralisation in the Morococha district, central Peru: mineralisation styles, timing and fluid evolution. Terre Environ 102:192

Catchpole H, Kouzmanov K, Fontboté L, Guillong M, Heinrich CA (2011) Fluid evolution in zoned Cordilleran polymetallic veins - Insights from microthermometry and LA-ICP-MS of fluid inclusions. Chem Geol 281:293–304. doi:10.1016/j.chemgeo.2010.12.016

Catchpole H, Kouzmanov K, Fontboté L (2012) Copper-excess stannoidite and tennantite-tetrahedrite as proxies for hydrothermal fluid evolution in a zoned Cordilleran base metal district, Morococha, central Peru. Can Mineral 50:719–743

Catchpole H, Kouzmanov K, Putlitz B, Fontboté L, Seo JH (2015) Zoned base metal mineralization in a porphyry system: Origin and evolution of mineralizing fluids in the Morococha district, Peru. Econ Geol 110:39–71

Centromin Perú (2002) Mapa Geológico del Distrito de Morococha, escala 1:10 000

Cherniak DJ, Watson EB, Grove M, Harrison TM (2004) Pb diffusion in monazite: a combined RBS/SIMS study. Geochim Cosmochim Acta 68:829–840

Chevalier A (2010) The Ticlio porphyry Cu-Au prospect, Morococha district, Peru: geochemistry and evolution of ore-forming fluids. unpublished Master thesis, University of Geneva

Chiaradia M, Schaltegger U, Spikings R, Wotzlaw J-F, Ovtcharova M (2013) How accurately can we date the duration of magmatic-hydrothermal events in porphyry systems?—An invited paper. Econ Geol 108:565–584

Condon DJ, McLean N, Noble SR, Bowring SA (2010) Isotopic composition ($^{238}U/^{235}U$) of some commonly used uranium reference materials. Geochim Cosmochim Acta 74:7127–7143

Dalrymple GB, Lanphere MA (1971) $^{40}Ar/^{39}Ar$ technique of K-Ar dating: a comparison with the conventional technique. Earth Planet Sci Lett 12:300–308

Cerro de Pasco Copper Corporation (1948) Lead and zinc deposits of the Cerro de Pasco Corporation in central Peru. In: 18th International Geological Congress, Great Britain. pp 154-186

Cerro de Pasco Copper Corporation (1965) Morococha ore inventory. Report:505

Deckart K, Silva W, Spröhnle C, Vela I (2014) Timing and duration of hydrothermal activity at the Los Bronces porphyry cluster: an update. Miner Deposita:1 - 12

Dilles J, Martin MW, Stein HJ (2003) Re-Os and U-Pb ages for the Butte copper district, Montana: a short- or long-lived hydrothermal system? Paper presented at the GSA 2003 Seattle Annual Meeting, Seattle

Eyzaguirre VR, Montoya DE, Silberman ML, Noble DC (1975) Age of igneous activity and mineralization, Morococha district, central Peru. Econ Geol 70:1123–1126

Faunes A, Hintze F, Siña A, Véliz H, Vivanco H (2005) Chuquicamata, core of a planetary scale Cu–Mo anomaly. In: Porter TM (ed) Super porphyry copper & gold deposits: a global perspective, vol 1. PGC Publishing, Adelaide, p 280

Guilbert JM, Park CFJ (1986) Deposits related to intermediate to felsic intrusions - cordilleran vein type deposits. In: Guilbert JM (ed) The geology of ore deposits, vol 4. W.H.Freemann and Company, New York, pp 465–487

Harris AC, Dunlap WJ, Reiners PW, Allen CA, Cooke DR, White NC, Campbell IH, Golding SD (2008) Multimillion year thermal history of a porphyry copper deposit: application of U-Pb, $^{40}Ar/^{39}Ar$ and (U-Th)/He. Miner Deposita 43:295–314

Harrison TM, Célérier J, Aikman AB, Hermann J, Heizler MT (2009) Diffusion of ^{40}Ar in muscovite. Geochim Cosmochim Acta 73:1039–1051

Hedenquist JW, Arribas AJ, Reynolds TJ (1998) Evolution of an intrusion-centered hydrothermal system: far Southeast-Lepanto porphyry and epithermal Cu-Au deposits, Philippines. Econ Geol 93:373–404

Hedenquist JW, Claveria RJR, Villafuerte GP (2001) Types of sulfide-rich epithermal deposits, and their affiliation to porphyry systems: Lepanto-Victoria-Far Southeast deposits, Philippines, as examples. Paper presented at the Pro-Explo 2001, Congreso Internacional de Prospectores y Exploradores, Lima

Houston RA, Dilles JH (2013) Structural geologic evolution of the Butte District, Montana. Econ Geol 108:1397–1424

Jaffey AH, Flynn KF, Glendenin LE, Bentley WC, Essling AM (1971) Precision measurement of half-lives and specific activities of ^{235}U and ^{228}U. Phys Rev Sect C 4:1889–1906

Kouzmanov K, Ovtcharova M, von Quadt A, Guillong M, Spikings R, Schaltegger U, Fontboté L, Rivera L (2008) U-Pb and $^{40}Ar/^{39}Ar$ age constraints for the timing of magmatism and mineralization in the giant Toromocho porphyry Cu-Mo deposit, Central Peru. In: XIII Congreso Latinoamericano de Geología, Lima, Peru.

Krogh TE (1973) A low-contamination method for hydrothermal decomposition of zircon and extraction of U and Pb for isotopic age determinations. Geochim Cosmochim Acta 37:485–494

León Pimentel J (2006) Relación espacial y temporal entre el sistema pórfido-skarn Toromocho y la sobreimpresión de las posteriores vetas cordilleranas de metales base. Tesis de Ingeniero Geólogo, Universidad Nacional de Ingeniería

Lepry LAJ (1981) The structural geology of the Yauli Dome region, Cordillera Occidental, Peru. unpublished Master thesis, University of Arizona

Lowell D, Alvarez A (2005) Deposito pórfido - Skarn de cobre - Toromocho. In: ProEXPLO'06. Minera Peru Copper Syndicate S.A.

Lund K, Aleinikoff JN (2005) Geochronologic evidence of multiple overlapping, fracture-controlled magmatic and hydrothermal pulses in the Butte district: genetic implications for Ag and Cu veins and porphyry Mo. Paper presented at the GSA 2005 Salt Lake City Annual Meeting, Salt Lake City

Lund K, Aleinikoff JN, Kunk MJ, Unruh DM, Zeihen GD, Hodges WC, du Bray EA, O'Neill JM (2002) SHRIMP U-Pb and $^{40}Ar/^{39}Ar$ age constraints for relating plutonism and mineralization in the Boulder Batholith region, Montana. Econ Geol 97:241–267

Maksaev V, Munizaga F, McWilliams M, Fanning M, Mathur R, Ruiz J, Zentilli M (2004) New chronology for El Teniente, Chilean Andes, from U/Pb, $^{40}Ar/^{39}Ar$, Re/Os and fission-track dating: implications for the evolution of a supergiant porphyry Cu deposit. Soc Econ Geol Spec Publ 11:15–54

Markey RJ, Hannah JL, Morgan JW, Stein HJ (2003) A double spike for osmium analysis of highly radiogenic samples. Chem Geol 200:395–406

Martin MW, Dilles JH, Proffett JM (1999) U-Pb geochronologic constraints for the Butte porphyry system. Paper presented at the Geological Society of America Annual Meeting

Masterman GJ, Cooke DR, Berry RF, Clark AH, Archibald DA, Mathur R, Walshe JL, Durán M (2004) $^{40}Ar/^{39}Ar$ and Re-Os geochronology of porphyry copper - molybdenum deposits and related copper - silver veins in the Collahuasi district, northern Chile. Econ Geol 99:673–690

McLaughlin DH, Graton LC (1935) Copper in the Cerro de Pasco and Morococha districts, Department of Junin, Peru. In: Copper resources of the world - XVI International Geological Congress, vol 2. pp 513-544

Mégard F (1984) The Andean orogenic period and its major structures in central and northern Peru. J Geol Soc Lond 141:893–900

Meyer C, Shea E, Goddard C, Staff (1968) Ore deposits at Butte, Montana. In: Ridge JD (ed) Ore deposits of the United States 1933-1967, vol 2. American Institute of Minerals, Metals, and Petroleum Engineers, New York, pp 1373–1416

Muntean JL, Einaudi MT (2000) Porphyry gold deposits of the Refugio district, Maricunga Belt, Northern Chile. Econ Geol 95:1445–1472

Muntean JL, Einaudi MT (2001) Porphyry-Epithermal transition: Maricunga Belt, Northern Chile. Econ Geol 96:743–772

Nagell RH (1960) Ore controls in the Morococha district, Peru. Econ Geol 55:962–984

Noble DC, McKee EH (1999) The Miocene metallogenic belt of central and northern Perú. In: Skinner BJ (ed) Geology and Ore Deposits of the Central Andes, vol 7. Society of Economic Geologists Special Publication. pp 155-193

Ojeda JM (1986) The Escondida porphyry copper deposit, II Region, Chile: Exploration drilling and current geological interpretation. In: Mining Latin America. Institution of Mining and Metallurgy, London, p 299−318

Ossandón G, Fréraut R, Gustafson LB, Lindsay DD, Zentilli M (2001) Geology of the Chuquicamata mine: a progress report. Econ Geol 96:242–270

Padilla Garza RA, Titley SR, Pimentel F (2001) Geology of the Escondida porphyry copper deposit, Antofagasta region, Chile. Econ Geol 96:307–324

Paliza R, Chavez WX (2008) Characterization of the alteration and mineralization of the Manto Italia orebody, Morococha District, Peru. In: XIII Congreso Latinoamericano de Geología, Lima

Parrish RR (1990) U–Pb dating of monazite and its application to geological problems. Can J Earth Sci 27:1431–1450

Peru Copper Inc. (2006) Annual Report 2006

Petersen U (1965) Regional geology and major ore deposits of central Peru. Econ Geol 60:407–476

Prendergast K, Clarke GW, Pearson NJ, Harris K (2005) Genesis of pyrite-Au-As-Zn-Bi-Te zones associated with Cu-Au skarns: evidence from the Big Gossan and Wanagon gold deposits, Ertsberg District, Papua, Indonesia. Econ Geol 100:1021–1050

Rainbow A (2009) Genesis and evolution of the Pierina high-sulphidation epithermal Au-Ag deposit, Ancash, Perú. unpublished PhD thesis, Queen's University

Renne PR, Swisher CC, Deino AL, Karner DB, Owens TL, DePaolo DJ (1998) Intercalibration of standards, absolute ages and uncertainties in $^{40}Ar/^{39}Ar$ dating. Chem Geol 145:117–152

Reynolds P, Ravenhurst C, Zentilli M, Lindsay D (1998) High-precision $^{40}Ar/^{39}Ar$ dating of two consecutive hydrothermal events in the Chuquicamata porphyry copper system, Chile. Chem Geol 148:45-60

Rivera N, Kobe HW (1983) Evolución geológica del Domo de Yauli. Bol Soc Geol Perú 72:159–175

Rosas S, Fontboté L, Tankard A (2007) Tectonic evolution and paleogeography of the Mesozoic Pucará Basin, central Peru. J S Am Earth Sci 24:1–24

Schandl ES, Gorton MP (2004) A textural and geochemical guide to the identification of hydrothermal monazite: criteria for selection of samples for dating epigenetic hydrothermal ore deposits. Econ Geol 99:1027–1035

Schärer U (1984) The effect of initial ^{230}Th disequilibrium on young U-Pb ages: the Makalu case, Himalaya. Earth Planet Sci Lett 67:191–204

Schmitz MD, Schoene B (2007) Derivation of isotope ratios, errors, and error correlations for U-Pb geochronology using ^{205}Pb-^{235}U-(^{233}U)-spiked isotope dilution thermal ionization mass spectrometric data. Geochem Geophys Geosyst 8:1–20

Schütte P, Chiaradia M, Barra F, Villagómez D, Beate B (2012) Metallogenic features of Miocene porphyry Cu and porphyry-related mineral deposits in Ecuador revealed by Re-Os, $^{40}Ar/^{39}Ar$, and U-Pb geochronology. Miner Deposita 47:383–410

Seedorff E, Dilles JH, Proffett JM, Einaudi MT, Zurcher L, Stavast WJA, Johnson DA, Barton MD (2005) Porphyry deposits: characteristics and origin of hypogene features. Econ Geol 100th Anniv Vol:251-298

Sillitoe RH (2010) Porphyry copper systems. Econ Geol 105:3–41

Sillitoe RH, Mortensen JK (2010) Longevity of porphyry copper formation at Quellaveco, Peru. Econ Geol 105:1157–1162

Sillitoe RH, McKee EH, Vila T (1991) Reconnaissance K-Ar geochronology of the Maricunga gold-silver belt, northern Chile. Econ Geol 86:1261–1270

Simmons AT, Tosdal RM, Wooden JL, Mattos R, Concha O, McCracken S, Beale T (2013) Punctuated magmatism associated with porphyry Cu-Mo formation in the Paleocene to Eocene of Southern Peru. Econ Geol 108:625–639

Smoliar MI, Walker RJ, Morgan JW (1996) Re-Os isotope constraints on the age of Group IIA, IIIA, IVA and IVB iron meteorites. Science 271:1099–1102

Snee L, Miggins D, Reed MH, Dilles JH, Zhang L (1999) Thermal history of the Butte porphyry system, Montana. In: Geological Society of America Annual Meeting. pp A-380

Stacey JS, Kramers JD (1975) Approximation of terrestrial lead isotope evolution by a two-stage model. Earth Planet Sci Lett 26:207–221

Steiger RH, Jäger E (1977) Subcommission on geochronology: convention on the use of decay constants in geo- and cosmochronology. Earth Planet Sci Lett 36:359–362

Stein HJ (2005) New model for the Butte Cu-Mo porphyry and polymetallic vein deposits, and the hosting Boulder batholith, SW Montana, USA. Geochimica et Cosmochimica Acta Supplement - Goldschmidt Conference Abstracts 2005 69:A566

Stein HJ (2014) Dating and tracing the history of ore formation. In: Holland HD, Turekian KK (eds) Treatise on geochemistry, 13 2nd edn. Elsevier, Oxford, pp 87–118

Stein HJ, Morgan JW, Scherstén A (2000) Re-Os dating of low-level highly-radiogenic (LLHR) sulfides: the Harnäs gold deposit, southwest Sweden, records continental scale tectonic events. Econ Geol 95:1657–1671

Stein HJ, Markey RJ, Morgan JW, Hannah JL, Scherstén A (2001) The remarkable Re-Os chronometer in molybdenite: how and why it works. Terra Nova 13:479–486

Terrones AJ (1949) La Estratigrafía del distrito minero de Morococha. Soc Geol Perú Volumen Jubilar, XXV Aniversario, Parte II:1-15

Trefzger EF (1937) Das Kupfererzvorkommen der Grube Morococha, Peru. Metall und Erz 34:181–192

von Quadt A, Erni M, Martinek K, Moll M, Peytcheva I, Heinrich CA (2011) Zircon crystallization and the lifetimes of ore-forming magmatic-hydrothermal systems. Geology 39:731–734

Zimmerman A, Stein HJ, Hannah JL, Kozelj D, Bogdanov K, Berza T (2008) Tectonic configuration of the Apuseni-Banat-Timok-Srednogorie belt, Balkans-South Carpathians, constrained by high precision Re-Os molybdenite ages. Miner Deposita 43:1–21